Journal of Structural Geology 32 (2010) 2072–2092

Contents lists available at ScienceDirect

Journal of Structural Geology

journal homepage: www.elsevier.com/locate/jsg

Review Article

Vorticity analysis in shear zones: A review of methods and applications

P. Xypolias*

Department of Geology, University of Patras, GR-26500, Patras, Greece

ARTICLE INFO

Article history:
Received 11 April 2010
Received in revised form
30 July 2010
Accepted 15 August 2010
Available online 24 August 2010

Keywords:
Vorticity number
Vorticity methods
Ductile flow
Monoclinic flow
Flow path

ABSTRACT

Quantitative vorticity analyses in naturally deformed rocks are essential for studying the kinematics of flow in shear zones and can be performed using a range of methods, which have been developed over the last two decades. The purpose of this review is to act as a starting point for the reader who needs a current overview of the existing methods and to indicate in what circumstances these methods can be most suitably applied. The review begins by providing an overview of deformation theory, followed by description of the most promising methods – in terms of assumptions, analytical procedures, and possible sources of uncertainty. Finally, the methods are compared on the basis of their uncertainties and strain memory, and discussed in terms of how they can be used to retrieve information about temporal and spatial variation of flow vorticity in shear zones. This review confirms that, although the existing methods are valuable, they are at an immature stage of development and suffer from limitations and uncertainties leading to interpretational problems, which, at present, can be alleviated by applying as many methods as possible to a given sample. Additional studies are recommended to advance the development of existing and new methods.

1. Introduction

Natural deformation is commonly concentrated into shear zones that range from the centimetre to the kilometre scale in width. Understanding the kinematics of flow in these zones is a prerequisite for elucidating critical aspects of the tectonic evolution of the Earth's crust, as well as for deciphering the kinematic significance of fabrics in deformed rocks. The ideal model of simple shear (Ramsay and Graham, 1970; Ramsay, 1980) has strongly influenced the thinking of structural geologists about the formation of high-strain zones and, for many years, it was a standard of reference for interpreting geological structures. Semi-qualitative studies during the decade of 80s inferred from crystallographic fabrics that the deformation path within some naturally occurring shear zones was not strictly progressive simple shear but included a pure shear component, emphasizing that it is more appropriate to interpret structures in terms of the degree of non-coaxiality rather than in terms of either perfectly non-coaxial or coaxial flow (Law et al., 1984, 1986; Platt and Behrmann, 1986). Such observations generated the necessity to find practical ways for determining the degree of non-coaxiality, or in other words, for evaluating the relation between the vortical and the stretching components of flow using numerical quantities such as the kinematic vorticity number (e.g. Truesdell, 1953; Means et al., 1980). The challenge was, and continues to be, the effective use of structural/fabric data to quantify kinematic flow, commonly referred to as *vorticity analyses*. Since the first vorticity analysis in naturally deformed mylonites by Passchier (1987a), significant progress in developing practical methods for vorticity analysis has been made by many geologists (Passchier and Urai, 1988; Wallis, 1992; Simpson and De Paor, 1993; Tikoff and Fossen, 1995; Grasemann et al., 1999; Holcombe and Little, 2001; Jessup et al., 2007; Gomez-Rivas et al., 2007; Johnson et al., 2009a; Xypolias, 2009), accompanied by numerous theoretical works about the kinematics of rock flow (e.g. Ghosh and Ramberg, 1976; Lister and Williams, 1983; Passchier, 1987b, 1997; Weijermars, 1991; Fossen and Tikoff, 1993; Jiang, 1999; Iacopini et al., 2010).

Especially in the last ten years, different vorticity analysis methods have been applied, either in isolation or in combination, to study shear zones from various tectonic settings (Xypolias and Doutsos, 2000; Bailey and Eyster, 2003; Law et al., 2004; Marques et al., 2007; Iacopini et al., 2008; Sullivan, 2008; Frassi et al., 2009; Xypolias et al., 2010; Law, 2010; Thigpen et al., 2010a). Such vorticity studies have confirmed that simple shear is the exception rather than the rule in natural deformation and have presented preliminary data about the temporal and/or the spatial variation of the vorticity of flow in natural shear zones. The identification of a pure shear component of deformation in a shear zone is critically important since during a persistent flow governed by a simultaneous combination of pure and simple shear, it is possible

* Tel./fax: +30 2610 994485.
E-mail address: p.xypolias@upatras.gr.

0191-8141/$ – see front matter © 2010 Elsevier Ltd. All rights reserved.
doi:10.1016/j.jsg.2010.08.009

to cause elongation of deforming material parallel to the walls of the zone (Wallis et al., 1993). It has been also shown that even for a relatively small pure shear component, this transport-parallel elongation can be significant if strain magnitude is enough (Xypolias and Kokkalas, 2006). Such observations, especially when they are combined with data about the spatio-temporal variation of flow vorticity, may shed light on the tectonic setting of the shear zone in question (e.g. Wallis et al., 1993; Northrup, 1996; Grujic et al., 1996; Grasemann et al., 1999; Law et al., 2004).

From the above, it becomes apparent that vorticity analysis is a relatively new and valuable tool for solving problems in structural geology and tectonics. However, due to the complexity of natural deformation, we have a fragile sense of confidence about numbers extracted from rocks using methods of vorticity analysis, which are still in a relatively immature stage of development. Therefore, apart from the analytical procedure, one must be aware of possible sources of error linked to the application of vorticity methods. In many application studies, however, the error is rarely discussed in detail. The purpose of this review is to present a state-of-the-art summary of current knowledge about vorticity analysis methods in terms of theoretical background, analytical procedure, limitations and possible sources of errors and uncertainties. Due to a limited database, a comprehensive comparison of existing methods is currently impossible but an attempt is made to discuss the consistency or discrepancies between various methods in the context of uncertainties and the length of strain memory associated with the different methods. This review begins with an overview of the basics of deformation theory.

2. Overview of theory

At any instant of time, the velocity field around a point in a deforming continuum can be described, with respect to a Cartesian coordinate system, by the flow or velocity gradient tensor, **L**, ($L_{ij} = \partial v_i/\partial x_j$; $i, j = 1, 2, 3$) and the related velocity gradient equation:

$$v_i = L_{ij}x_j \tag{1}$$

where v_i is the velocity at spatial coordinate x_j (Malvern, 1969; Ramberg, 1975). If **L** is space-independent and remains unvarying throughout the deforming volume of material, the flow is considered to be *homogeneous*, otherwise the flow is *heterogeneous*. Also, the flow is considered to be *steady* if **L** is time-independent, otherwise it is *non-steady*. The vast majority of analytical works in the geological literature are limited to homogeneous and steady-state flows mainly because their mathematical description is simple. Notice, for example, that homogeneous flows have linear velocity gradients and can be described in a straightforward manner while heterogeneous flows have non-linear velocity gradients, which require application of numerical integration methods of governing equations for their description. However, it is widely accepted that deformation in nature is generally heterogeneous and non-steady. The problem of heterogeneity can be partly overcome by subdividing the deforming continuum into smaller domains where the flow can be approximately viewed as homogeneous. The assumption of steadiness of flow, however, remains a fundamental problem since little is known about flow paths in progressive deformation. Thus, for the present state of knowledge, homogeneous steady-state flows represent a valuable standard of reference for investigating more complex natural systems.

2.1. Decomposition of the flow tensor

The flow tensor can be decomposed into the symmetric tensor **D** and the anti-symmetric tensor **W**, which are related to the stretching and the vortical (or rotational) components of velocity field, respectively (Malvern, 1969; Ramberg, 1975; McKenzie, 1979; Lister and Williams, 1983):

$$\mathbf{L} = \mathbf{D} + \mathbf{W} \tag{2}$$

Note that the flow tensor does not contain the translating component of the velocity field. This component vanishes by fixing the coordinate system to the particle in question.

The symmetric quantity **D** is the stretching tensor and its three orthogonal eigenvectors are known as the Instantaneous Stretching Axes, ISA_i ($i = 1, 2, 3$), of flow. The eigenvalues of **D** describe the stretching rates, s_i (i = a, b, c), of material lines instantaneously parallel to these axes and can have any magnitude. For planar deformation zones in isotropic material, the ISAs are thought to be parallel to the stress axes (Weijermars, 1991).

The anti- (or skew-) symmetric part **W** is the vorticity tensor and describes, with respect to a coordinate system, the angular velocities (ω) of local elements (lines or particles) of a deforming body without their stretch. Since the vorticity tensor is skew-symmetric, it can be simply expressed by a vector called the *vorticity vector* (**w**), the magnitude (or length) of which defines the vorticity, **w**, of flow. Strictly mathematically, the vorticity vector is the curl of velocity ($\mathbf{w} = \mathrm{curl}v_i$), which is also equal to twice the angular velocity vector ($\mathbf{w} = 2\boldsymbol{\omega}$) (e.g. Malvern, 1969, p.147; Means et al., 1980). The plane lying normal to these vectors is known as *Vorticity Profile Plane* (VPP; Robin and Cruden, 1994) or *Vorticity Normal Section* (Jiang and Williams, 1998) (Fig. 1a). Different interpretations of the physical meaning of vorticity have been made by various authors (Means et al., 1980; Ghosh, 1987; Means, 1994; Tikoff and Fossen, 1995) and generally it can be thought of as (Fig. 1a): (1) equal to the sum of the angular velocities of any pair of instantaneously orthogonal material lines in the VPP; (2) twice the average angular velocity of all material lines lying in the VPP and passing through a particle in question; or (3) twice the rate of rotation of a rigid spherical particle in a ductilely deformed matrix. Moreover, flows with vorticity are said to be *rotational*, otherwise the flows are said to be *irrotational*.

The orientation of the vorticity vector with respect to the three orthogonal ISAs controls the symmetry of flow but, theoretically, no unique angular relationship exists between these directions. In simple flow types, the vorticity vector remains parallel to one of the ISAs. Such flow types have a monoclinic or higher symmetry, and are referred to as *monoclinic flows* (Fig. 1a) (Passchier, 1998). If the vorticity vector is oblique to all ISAs, the flow is said to be *triclinic* (Fig. 1b) (Robin and Cruden, 1994). Flows with monoclinic symmetry are admittedly an end-member case, but several examples show that such flows are not uncommon in natural shear zones. In most examples, the relation $s_b > s_a$ and $s_b > s_c$ exists between the instantaneous stretching rates, while the vorticity vector lies parallel to ISA_3 (Fig. 1a).

2.2. Vorticity decomposition

The magnitude and orientation of **w** can vary according to the framework chosen as a reference frame. It has been recognized and extensively discussed by several authors (Means et al., 1980; Lister and Williams, 1983; Jiang, 1999) that the vorticity can be decomposed, with respect to an external (often geographical) reference frame, into: (1) an “internal” or shear-induced vorticity (w_i), which represents the rotation of material lines with respect to the ISAs; and (2) a vortical component, known as spin (or external spin), which results in rotation of ISAs (and all lines) through the external reference frame. The concept of vorticity

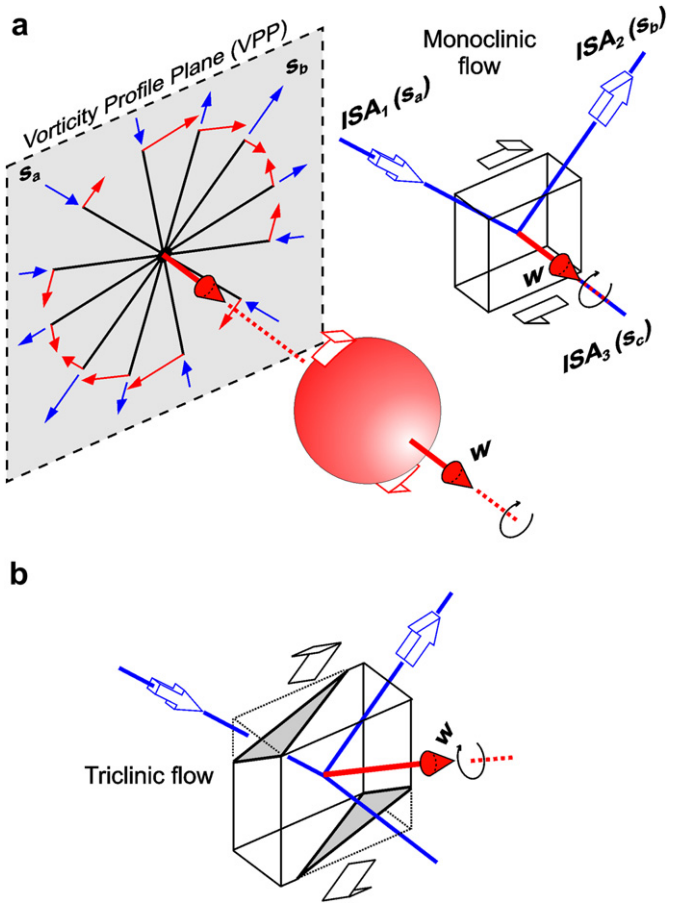

Fig. 1. (a) Orientation of vorticity vector, w, with respect to the $ISA_{1,2,3}$ (Instantaneous Stretching Axes) for a monoclinic flow, and its relation to the instantaneous angular velocities (red arrows) of material lines as well as to a rotating spherical particle. The sense of stretching rate (blue arrows) of material lines with respect to ISA is also shown; $s_{a,b,c}$ – principals stretching rates. (b) In triclinic flow types the vorticity vector is oblique to all ISAs. (For interpretation of the references to colour in this figure legend, the reader is referred to the web version of this article.)

decomposition can be visualised by considering a planar shear zone that is subjected to homogeneous steady-state deformation and coevally rotates in a randomly chosen external references frame (Fig. 2). The geometry of rock fabrics in the shear zone is influenced by the internal vorticity and reflects the flow type, which can be *non-coaxial* if the material lines continuously diverge from the orientation of the ISAs or *coaxial* if lines parallel to the ISAs do not rotate relative to these axes. Thus, vorticity measured with respect to a material marker (i.e. shear zone boundary; Fig. 2) that serves as an internal reference system, is the internal vorticity and is caused by the non-coaxial component of deformation. The rotation, in turn, of both the ISAs and the shear zone as a whole is the product of spin, which is equivalent to the rotation of a rigid-body about an axis. The spin component has no effect on the geometry of fabrics, and therefore cannot remove the non-coaxiality (e.g. Means, 1994). Moreover, it is hard or even impossible to determine the amount of rotation of a shear zone. Hence, it is more convenient and useful for describing vorticity to attach the reference frame to a material marker (Weijermars, 1991; Simpson and De Paor, 1993; Tikoff and Fossen, 1995) or alternatively to use a reference frame that remains at fixed angle or parallel to the ISAs (Passchier, 1987b, 1997, 1998; Iacopini et al., 2007). The latter reference frame simplifies the flow description because the spin component vanishes.

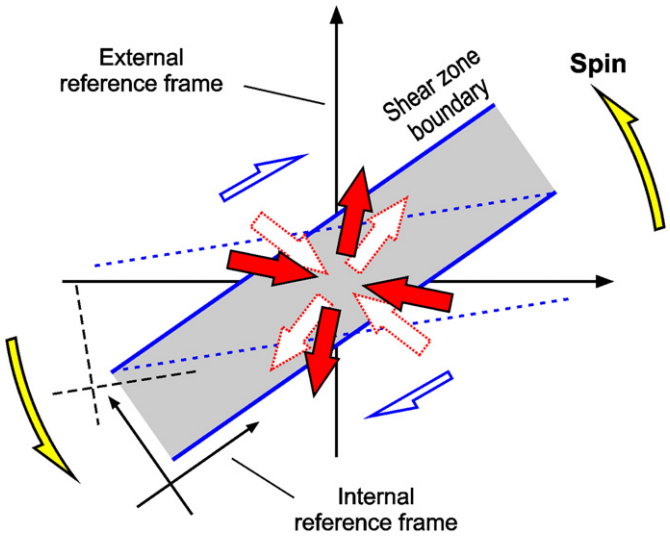

Fig. 2. Illustration of the vortical component, known as spin, which results in rotation of both the ISAs (red arrows) and the shear zone through an external reference frame. Dash lines –orientation of ISA and shear zone before rotation; solid lines – after rotation. Vorticity measured with respect to an internal reference frame is the internal vorticity. (For interpretation of the references to colour in this figure legend, the reader is referred to the web version of this article.)

2.3. Dimensionless vorticity measures

The *kinematic vorticity number*, W_k, was defined by Truesdell (1953) and introduced into the geological literature by Means et al. (1980) as a measure of the degree of instantaneous non-coaxiality of flow. This non-dimensional number normalizes the internal vorticity, w_i, to the magnitude of principals instantaneous stretching rates, s_i, as follow:

$$W_k = w_i\left[2\left(s_a^2 + s_b^2 + s_c^2\right)\right]^{-1/2} \quad (3)$$

The W_k has values equal or greater than 0, and flow with $W_k = 0$ is said to be coaxial. Thus, the degree of non-coaxiality increases with increasing W_k values.

For three-dimensional flows with monoclinic symmetry, less complex vorticity numbers than in Eq. (3) can be designated because the flow can be effectively described on the VPP (e.g. Passchier, 1988a,b; Weijermars, 1991; Tikoff and Fossen, 1993; Robin and Cruden, 1994). Thus, if the vorticity vector is parallel to ISA_3 (Fig. 1a) then a *sectional kinematic vorticity number*, W_n, can be defined as follow (Passchier, 1997):

$$W_n = w/2s_m \quad (4)$$

where w is the magnitude of vorticity vector and s_m is the mean stretching rate ($=(s_b - s_a)/2$). For formalizing monoclinic flows, Passchier (1997, 1998) defined also the *sectional kinematic dilatancy number*, $A_n(=(s_a + s_b)/2s_m)$, which describes the instantaneous area change in the VPP, as well as the *sectional kinematic extrusion number*, $T_n(=s_c/2s_m)$, which represents the elongation rate parallel to the vorticity vector. Remember that these sectional dimensionless numbers were designated by fixing the ISAs to the external reference frame. Therefore, strictly speaking, the W_n is a measure of the degree of rotationality of flow. For non-spinning flows, the W_k is related to W_n by the equation:

$$W_n = W_k\sqrt{2T_n^2 + A_n^2 + 1} \quad (5)$$

Thus, for plane strain ($T_n = 0$) equal-area ($A_n = 0$) deformation, $W_n = W_k$.

Another measure of instantaneous non-coaxiality for plane strain equal-area flows is the quantity S_r, which is defined as the ratio of the instantaneous pure shear strain rate (parallel to the direction of shearing) to the simple shear strain rate ($S_r = \dot{\epsilon}_x/\dot{\gamma}$; Ghosh and Ramberg, 1976), and is related to W_k ($=W_n$) by the equation (Ghosh, 1987):

$$S_r = \sqrt{\left(1 - W_k^2\right)}/2W_k \quad (6)$$

For plane strain deformation, W_k can also be expressed in the form (Tikoff and Fossen, 1993; Fossen and Tikoff, 1993):

$$W_k = \cos\left[\tan^{-1}(2\ln k/\gamma)\right] \quad (7)$$

where γ is the shear strain and k the elongation parallel to shear direction.

2.4. Particle movement paths

One of the most powerful properties of the kinematic numbers is their ability to characterize the geometry of particle paths for individual flow types. Particle paths (or streamlines) are open-ended or closed curves which represent the progressive change in position of particles during deformation. The most well known particle paths are those studied by Ramberg (1975) for the special regimes of two-dimensional (2D), steady-state and *non-dilatant* (equal-area, $A_n = 0$) flows such as (Fig. 3): pure shear ($W_n = 0$); general shear or sub-simple shear (De Paor, 1983) ($0 < W_n < 1$); simple shear ($W_n = 1$); super-simple shear (De Paor, 1983) ($1 < W_n < \infty$) and rigid-body or pure rotation ($W_n = \infty$). Passchier (1991, 1997) described a variety of 2D *dilatant flows* ($A_n \neq 0$) for varying W_n values; some of which are illustrated in Fig. 3. As a whole, the streamline patterns of both dilatant and non-dilatant 2D flow types can be categorized into: hyperbolic types; parallel types; elliptical or circular closed loops; and inward or outward radiant directed flow types (Fig. 3) (e.g. Passchier, 1997). Hyperbolic and elliptical streamline patterns are also considered to represent non-pulsating and pulsating deformation histories, respectively (Ramberg, 1975; McKenzie, 1979; Weijermars, 1991).

A remarkable feature of hyperbolic flow patterns (e.g. pure and general shear) is a set of two straight streamlines. These straight lines are asymptotes to the hyperbolas and define material lines that do not rotate with respect to the ISAs during progressive deformation. Axes in space that are parallel to such irrotational lines correspond to the eigenvectors of tensor **L** and for non-spinning flows they are known as *flow apophyses* (A_i; Fig. 3) (Ramberg, 1975; Passchier, 1986). Non-hyperbolic dilatant flow types with $W_n \leq 1$ also contain two separate or joined apophyses (Fig. 3), except for some cases with extremely large (positive or negative) A_n values. Moreover, pulsating flows do not have apophyses, but their streamline patterns are governed by imaginary lines, which can be considered as "ghostvectors" (Fig. 3) (Iacopini et al., 2007, 2010).

The apophyses control the flow geometry and for hyperbolic flow types, they can be recognized as extensional (A_2) or shortening (A_1) depending on whether they "attract" or "repulse" the material lines (or points) in a flow, respectively. For that reason, in geological applications the extensional apophysis, A_2, is assumed to be parallel to the boundaries of elongating shear zones (Fig. 4a) while the shortening apophysis, A_1, is parallel to the boundaries of contracting shear zones (Fig. 4b). In such cases, the apophysis defining the flow/shear plane is referred to as stable whilst the other is unstable or inclined. Also, apophysis A_2 is often referred to as the *fabric attractor* of flow (Passchier, 1997).

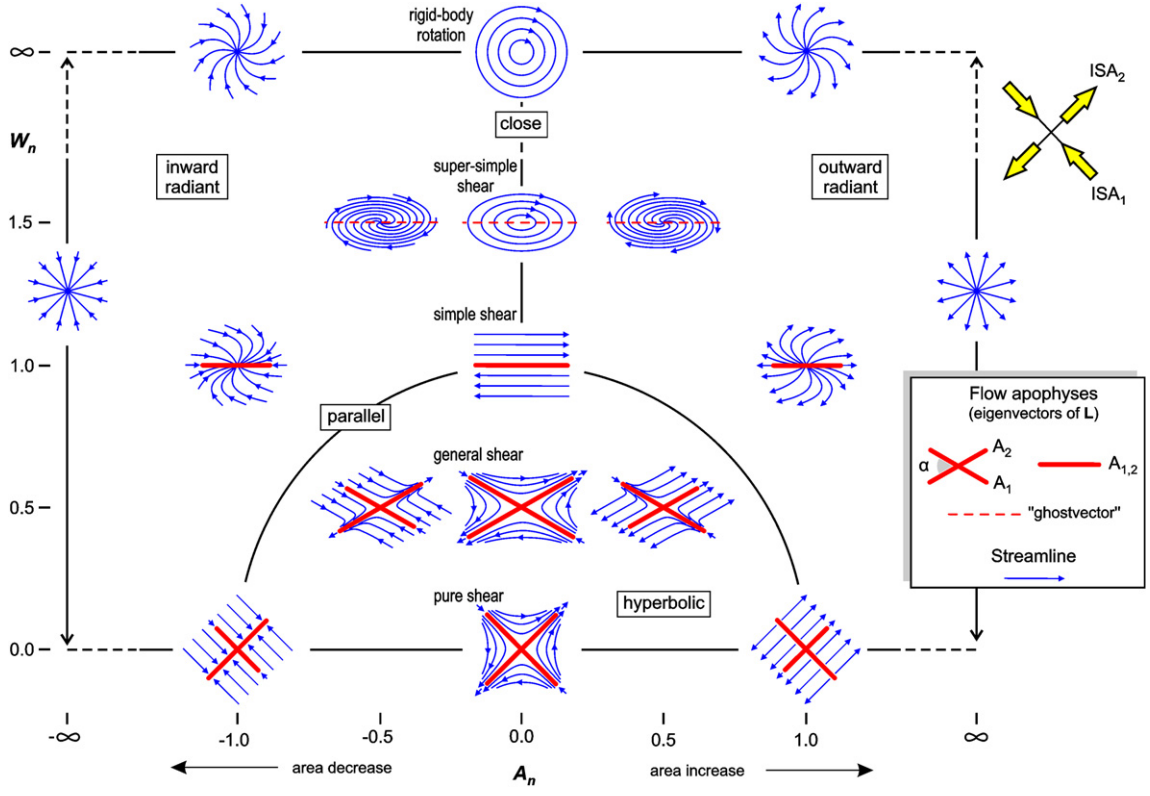

Fig. 3. W_n–A_n plane illustrating streamline patterns for representative two-dimensional steady-state flows (after Ramberg, 1975; Passchier, 1997). The orientation of instantaneous stretching axes, ISA (top right), for all flow types is the same. A general categorization of flow types according to shape of streamline patterns is also shown (after Passchier, 1997).

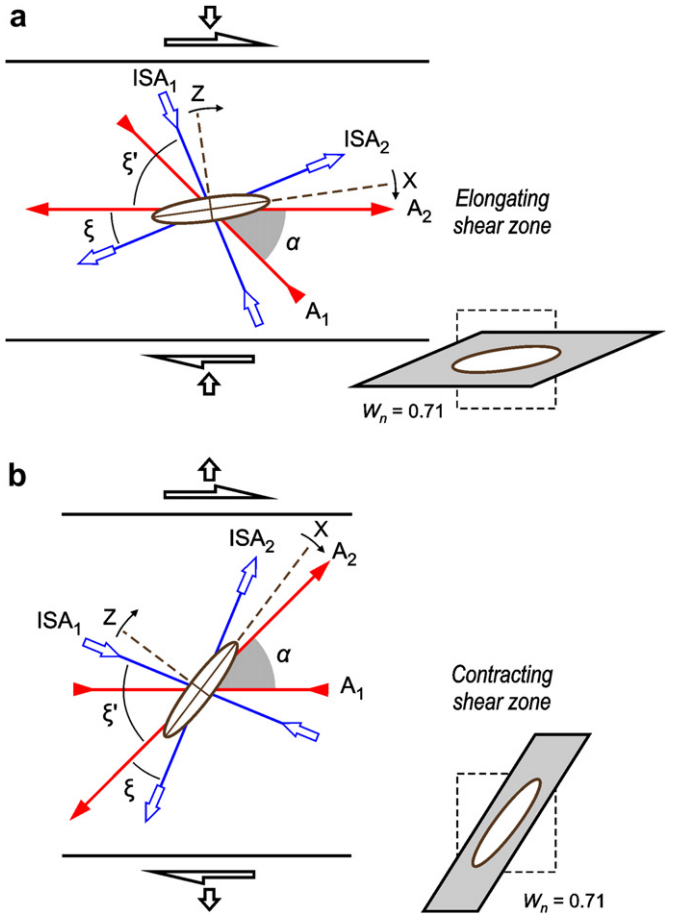

Fig. 4. Simplified sketch showing orientation of the instantaneous flow elements and their angular relationships in a dextral elongating (a) and a dextral contracting (b) general shear zone with $W_n = 0.71$. A_1 and A_2 – flow apophyses; ISA_1 and ISA_2 – instantaneous stretching axes; X and Z – principal strain axes. The vorticity vector lies perpendicular to the page.

The angle, α, between the flow apophyses (Figs. 3 and 4) always ranges between 0° and 90° and depends only on W_n as follows (Bobyarchick, 1986; Passchier, 1986):

$$W_n = \cos\alpha. \tag{8}$$

Thus, the flow apophyses are orthogonal for pure shear flow; form acute angles for general shear flow while for the special case of simple shear they coincide (Fig. 3). Moreover, Eq. (8) reveals that W_n is a non-linear measure of flow vorticity (e.g. Tikoff and Fossen, 1995). The intermediate case between pure and simple shearing occurs at $W_n = 0.71$ ($\alpha = 45°$) and not at $W_n = 0.5$ ($\alpha = 60°$) (Law et al., 2004). Furthermore, the extensional ISA_2 and the shortening ISA_1 form an angle ξ and ξ', respectively, with the extensional apophysis A_2 (Fig. 4a and b). Thus,

$$W_n = \sin 2\xi = \sin 2\xi' \tag{9}$$

(Weijermars, 1991). Eqs. (8) and (9) are extensively used in many vorticity analysis methods but both are strictly valid only for 2D flows (e.g. Tikoff and Fossen, 1995).

2.5. Representation of flow tensor in Mohr circle

The graphical representation of 2D homogeneous flows on Mohr circle diagrams was first introduced into the geological literature by Lister and Williams (1983; following J.P. Platt) and its usefulness has been demonstrated in numerous studies (Means, 1983; Passchier, 1987b, 1991; Bobyarchick, 1986; Grasemann et al., 2006; Coelho and Passchier, 2008). Here, the general properties of Mohr circle for flow tensor are presented. Some examples of equal-area flow types in real space and their corresponding representation in Mohr space are illustrated in Fig. 5a.

For a given flow type, the Cartesian coordinates of each point on Mohr circle represent the instantaneous angular velocity (ω) and the stretching rate (s) of a particular material line that lies in the VPP. Therefore, each circle contains infinite pairs of ω–s values which correspond to lines of all possible orientations through a given point. For equal-area flows, the centre of the circle lies on the ω-axis and its vertical distance from the s-axis is equal to half of vorticity. As a result, the Mohr circle for pure shear is centred on the origin of the axes (Fig. 5a). Circle radius is equal to the mean stretching rate (s_m) and thus pure rotational flows are plotted as points on the ω-axis (Fig. 5a). Furthermore, eigenvectors of both tensors **D** and **L** can be represented on the Mohr circle. Specifically, lines instantaneously parallel to ISAs, plot as anti-diametrical points on the circle and at equal distances from the abscissa axis (Fig. 5a). For pure shear and general shear, the flow apophyses (A_1, A_2) are represented by the intersections of Mohr circle with the s-axis (Fig. 5a). Note that the angle, α, between the two apophyses on the circle is twice the angle in real space. For simple shear, the joined apophyses plot at the unique point where the circle transects the abscissa. Also, the Mohr circle intersects the ω-axis at Ω_1 and Ω_2, which represent the directions of maximum and minimum angular velocities of material lines (Fig. 5a). In real space, these directions bisect the angle between A_1 and A_2 as well as the right angles defined by ISA_1 and ISA_2. For equal-area flows, these directions also coincide with the axes of zero stretching rates L_1 and L_2 (Fig. 5a).

Steady-state flows with area change can also be presented on Mohr circle, but in this case the circle's centre shifts parallel to the s-axis either leftward or rightward depending on if the area decreases ($A_n < 0$) or increases ($A_n > 0$), respectively, during progressive deformation (Fig. 5b). The cosine of the angle between L_1 and L_2, in real space, gives the A_n (Fig. 5c) (Passchier, 1991):

$$A_n = \cos\left(L_1 \hat{} L_2\right) \tag{10}$$

The horizontal distance of the Mohr circle centre from the ω-axis defines the rate of area change ($=s_a + s_b$).

2.6. Finite deformation

For a steady-state flow, the orientations of ISAs and flow apophyses with respect to a reference frame remain constant throughout deformation history. In response to this deformation, the material lines stretch and rotate tending to approach the extensional apophysis. Thus, the shape and orientation of any material line in the finite state of deformation are controlled by W_n, the finite strain as well as the bulk volume change. The position gradient tensor (or deformation gradient tensor), **F**, (Means, 1983; Bobyarchick, 1986; Passchier, 1988a; Tikoff and Fossen, 1993, 1995) contains information for all these parameters and can effectively describe finite deformation. In fact, the tensor **F** relates the position of material particles in the undeformed state to their position in the deformed state and is derived from the flow tensor **L** by the relation:

$$\mathbf{F} = \exp(\mathbf{L}t) \tag{11}$$

(see Passchier, 1988a for a full mathematical description). Representation of **F** in Mohr circle space (Means, 1982; De Paor

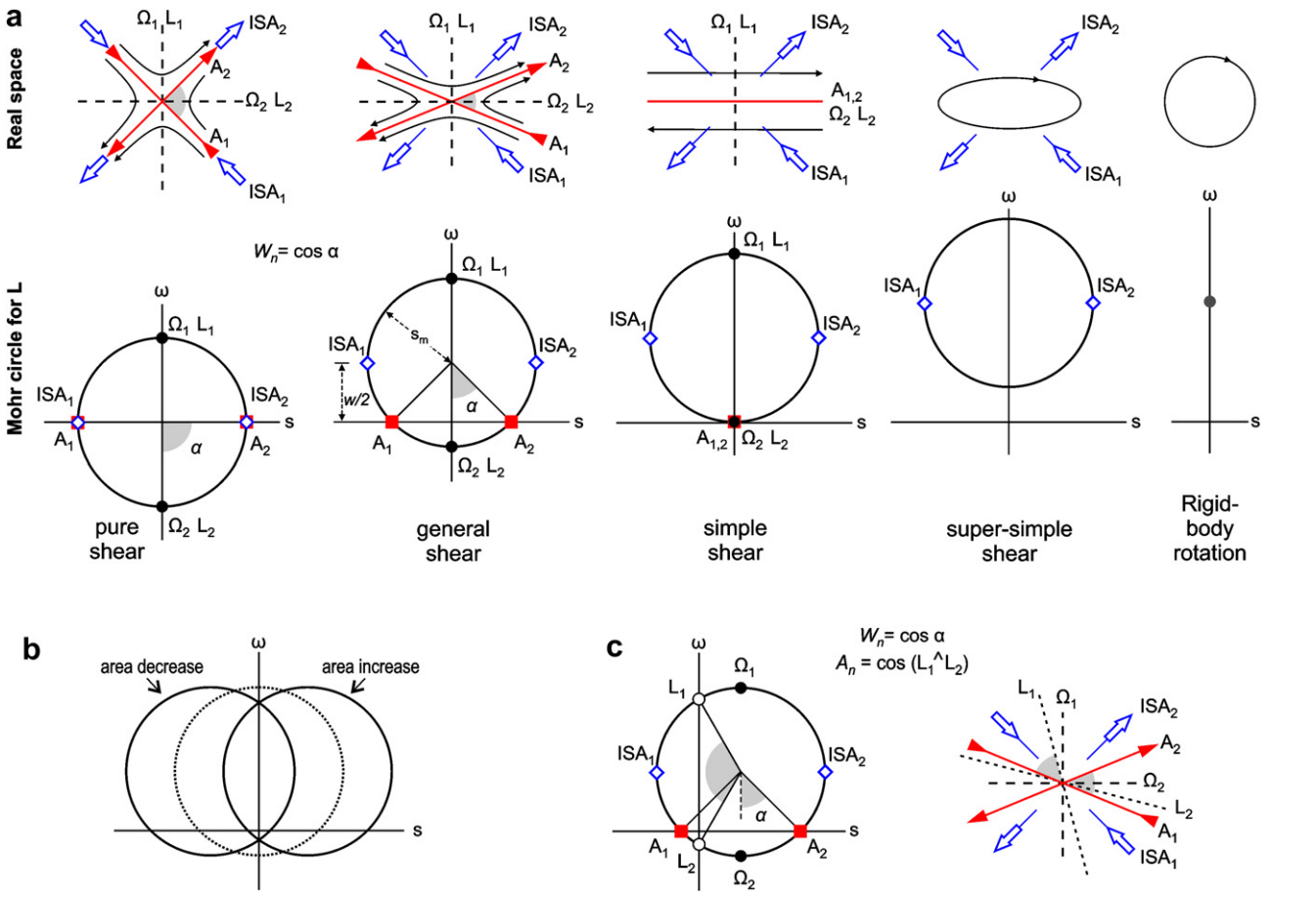

Fig. 5. (a) Instantaneous elements of steady-state equal-area flows in real space and their representation by Mohr-circles for the velocity gradient tensor, **L**. A_1 and A_2 – flow apophyses; ISA_1 and ISA_2 – instantaneous stretching axes; L_1 and L_2 – axes of zero stretching rates; Ω_1 and Ω_2 – directions of maximum and minimum angular velocities of material lines, respectively. Each point on the Mohr circle represents the instantaneous angular velocity, ω, and the stretching rate, s, of a particular material line. w – vorticity; s_m – mean stretching rate. (b) The position of Mohr circle (for **L**), with respect to the ω-axis for flows with area change. (c) The elements of a dilatant (area increase) flow in real space and their representation by Mohr-circles for **L**.

and Means, 1984; Passchier, 1988a, 1990a) is a powerful tool to describe finite deformation in planes parallel to VPP and has been used in many studies to establish methods of vorticity analysis (e.g. Passchier and Urai, 1988; Vissers, 1989; Passchier, 1990b; Wallis, 1992, 1995; Xypolias, 2009). Below, the properties and the construction method of Mohr circle analysis for **F** are given. Before that, it should be noted that a similar method is used to construct the Mohr circle for the reverse tensor of **F**, referenced as **H** (e.g. Passchier, 1990b). The latter tensor relates the particles position in the deformed state to the undeformed state. Moreover, for the sake of simplicity the following discussion is restricted to deformation paths produced by steady-state flows. However, the hypothesis of steadiness of deformation seems to be unrealistic in many natural shear zones. For that reason, and due to the instantaneous nature of W_n, calculations of rotational components of finite deformation can be more appropriately performed using the *mean kinematic vorticity number*, W_m, which represents a temporal average quantity of W_n. If flow in the deformation increment(s) of interest has been steady-state, then $W_n = W_m$.

The Mohr circle for tensor **F** (2×2) is plotted as an off-axis circle in stretch space. The polar coordinates of any point on the circle represent the rotation and stretch of material lines in real space (Fig. 6a) (Means, 1982; Passchier, 1988a). The angle between two points on the **F**-Mohr circle is twice the original angle between the corresponding lines in real space (e.g. α and ρ in Fig. 6a). The angle between two lines in the deformed state cannot be read from the Mohr circle, but can be calculated from the original angle between the lines and the amount of rotation for each line (e.g. ρ' in Fig. 6a). Intersection points of the circle with the horizontal axis represent material lines of zero finite rotation. These lines coincide with the flow apophyses at any instant during steady deformation histories. The finite strain axes plot at opposite ends of the diameter, which extends through the axes origin (Fig. 6a and b).

Generally, the values of three parameters are required to construct the Mohr circle for that final state of deformation: the radius R of the circle; the distance T of the circle centre from the axes origin; and the vertical distance, Q, of circle centre from the horizontal axis (Fig. 6b). For equal-area deformation, the parameters R and T are functions of strain ratio in the XZ plane of finite strain, R_{XZ}, only but they can modified to incorporate the finite area change, ΔA (Fig. 6b). The parameter Q depends on R and W_m as follows:

$$W_m = Q/R \tag{12}$$

Thus, $Q = 0$ for pure shear and $Q = 1$ for simple shear.

Progressive steady-state deformation with $0 \leq W_n \leq 1$ can be represented in Mohr space by a series of circles with increasing diameter, the centre of which translate along the abscissa axis for progressive pure shear or into the space for both progressive general and simple shear (Fig. 6c) (Passchier, 1988b).

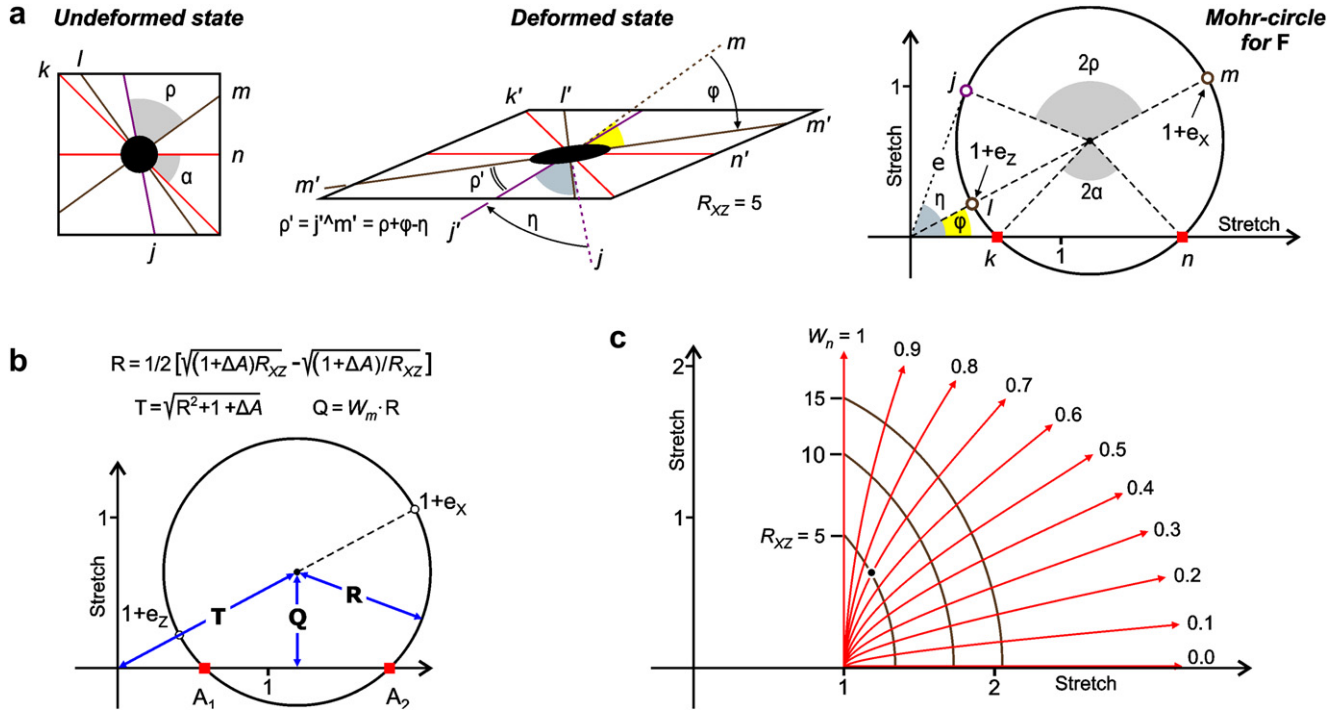

Fig. 6. Properties of the Mohr circle for the position gradient tensor, F (modified after Passchier, 1988a,b). (a) Representation of finite deformation in real space and in Mohr space. φ and η – angles of rotation of material lines m and j, respectively; ρ and α – angle between material lines in the undeformed state; ρ' – in the deformed state. The stretch and rotation of any material line plot as polar coordinates in Mohr space (e.g. e, η for line j). (b) Illustration of **F**-Mohr circle's parameters *R*, *T* and *Q* in terms of the finite strain ratio, $R_{XZ}[=(1+e_X)/(1+e_Z)]$; the finite area change, $\Delta A[=(1+e_X)(1+e_Z)-1]$; and the mean kinematic vorticity number, W_m. (c) Translation of **F**-Mohr circle's centre for various W_n values during steady isochoric deformation. Point on the diagram represents the circle centre in (a).

3. General limitations and assumptions of vorticity analysis

The above theoretical description is selectively focused on 2D flows where the vorticity vector and one of the ISAs are parallel to each other and both are perpendicular to the plane in question, the VPP. This focus is because the methods applied for estimating W_m (or W_n) utilize data collected on the XZ plane of the finite strain (parallel to lineation and normal to foliation), assuming monoclinic flow with the vorticity vector approximately parallel to the *Y*-axis of the strain ellipsoid. This assumption is reasonable for shear zones where vorticity gauges such as crystallographic fabrics, C- and C′-shear bands exhibit monoclinic (or orthorhombic) geometry with their symmetry axis being within the foliation and normal to lineation. However, a number of works (Lin et al., 1998; Jones and Holdsworth, 1998; Jiang and Williams, 1998; Iacopini et al., 2007; Forte and Bailey, 2007; Fernández and Díaz-Azpiroz, 2009) have inferred that shear zones can also be developed by flows with triclinic symmetry. Also, some studies (e.g. Jiang and Williams, 1998; Jiang et al., 2001) consider the monoclinic flow to be the exception rather than the norm in high-strain zones and have shown that triclinic flows with large simple shear components can theoretically produce structures with apparent monoclinic geometry. In such cases, the VPP is not necessary perpendicular to the symmetry axis of fabrics and such vorticity estimates from such fabrics are not accurate. In fact, no strict criteria exists to distinguish monoclinic from triclinic shear zones (Jiang and Williams, 1998; Passchier and Coelho, 2006). However, if both the lineation and the pole to foliation lie in a plane, which is oriented parallel to outcrops containing the best developed asymmetric structures (e.g. Czeck and Hudleston, 2003), then this plane is often assumed to be the VPP of a common monoclinic shear zone. For monoclinic elongating shear zone, the intersection between the main foliation and the zone boundary is also normal to VPP (Jiang and Williams, 1998).

Another limitation of 2D vorticity analysis is the assumption of plane strain deformation. For non-plane-strain deformation, no simple relationships exists between ISAs and flow apophyses and thus relations like Eqs (8) and (9) used by various methods for estimating W_m are not valid. However, Tikoff and Fossen (1995) investigated the effect of the third stretching direction (*Y*-axis) on vorticity estimates and demonstrated that the 2D analysis overestimate the 3D vorticity number by only a small amount. Specifically, the overestimation is expected to be around 0.05 for a vorticity number close to 0.6 and reduces to zero with increasing pure or simple shear component.

Deformation in lithological heterogeneous shear zones can lead to partitioning of flow between layers with differing competence. In such cases, vorticity number can vary from layer to layer even though the bulk geometry of flow remains constant during progressive deformation. For example, Lister and Williams (1983) suggested that competent layers tend to deform more coaxially than incompetent layers, although numerical models (Ishii, 1992; Jiang, 1994) have shown that this suggestion only holds for extremely competent domains (zero competence factor; see Jiang (1994) for details). Possibly, this problem can be addressed by performing vorticity analyses on samples collected from thick lithologically homogeneous horizons. The latter tend to deform in a manner similar to the whole system (Ishii, 1992). Moreover, for a thickness ratio (competent/less competent layers) ranging from 1/3 to 3 no noticeable effects on vorticity number are expected (Ishii, 1992).

4. Methods of vorticity analysis

This section provides an overview of the most commonly used methods for estimating W_m or W_n. Some methods rely on the same structural criterion and for that reason the section is organized in

terms of vorticity gauges. All methods are 2D so all descriptions refer to the plane of observation that is parallel to the XZ plane of the finite strain. Moreover, the description is restricted to elongating shear zones assuming that the extensional apophysis A_2 is parallel to the shear plane. Similar methodological approaches could be also used to analyse vorticity in contracting shear zones. Also, the application of some vorticity methods requires independent estimates of strain ratio R_{XZ}. Reviews of available techniques of strain analysis are given by Ramsay and Huber (1983) and Lisle (1994).

4.1. Deformed sets of veins or dykes

The stretch behaviour of a particular material line in a homogeneous deformed body is governed by the initial orientation of the line, the finite strain, volume change and W_m, and can be characterized by continuous extension (e), continuous shortening (s) or shortening followed by extension (se) and vice versa (es) (Talbot, 1970; Hutton, 1982; Ramsay and Huber, 1983; Passchier, 1986). In naturally occurring shear zones information about the stretch history of individual material lines can be retrieved by the deformation pattern of competent veins or dykes (i.e. boudinaged folds; Fig. 7a) of various orientations, provided that they are embedded in the host rock mainly before the onset of deformation. Utilizing the observation that sets of material lines with similar stretch histories occupy distinct geometric sectors in circular orientation diagrams, Passchier (1990b) proposed a method for estimating all finite deformation parameters including W_m, which is summarized below. Examples of the application of these method to naturally deformed rocks have been given by Passchier (1986), Passchier and Urai (1988), Wallis (1992), Kumerics et al. (2005) and Short and Johnson (2006).

Commonly, three types of material line sectors with different stretch histories can be distinguished on an orientation diagram: (s), (e), and (se) sectors. For steady-state flows, the distribution and the boundaries of these sectors are controlled by the orientation of material lines that lie parallel to the axes of zero stretching rates (L_1, L_2; Figs. 5 and 7a) at the onset of deformation and at the final

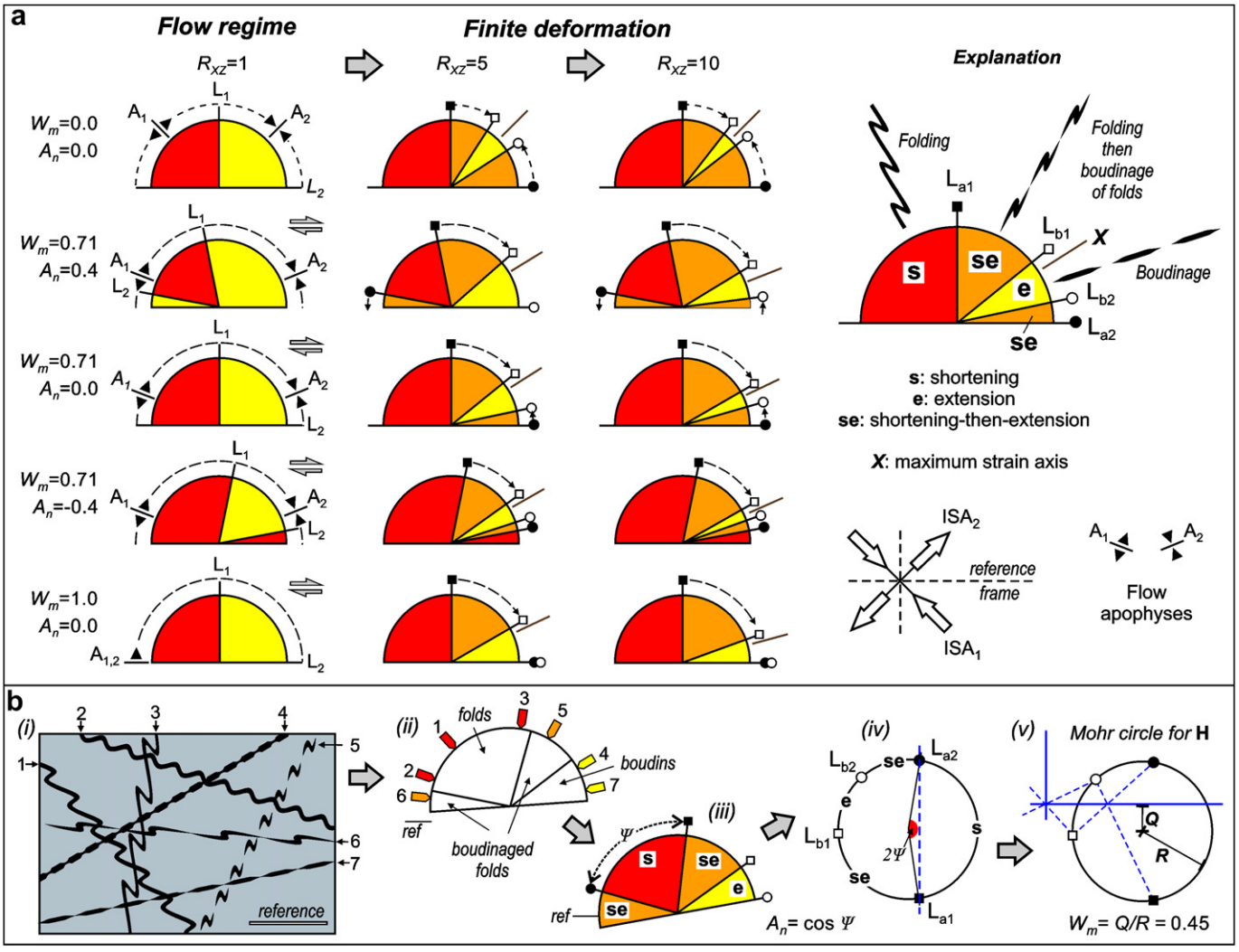

Fig. 7. (a) Diagrams illustrating the effects of W_m, A_n and R_{XZ} on the distribution and the size of sectors of material lines (i.e. deformed veins or dykes) with different stretch histories in real space during progressive deformation. The diagrams are valid for constant flow parameters (e.g. $W_m = W_n$). In incremental strain ($R_{XZ} = 1$), the axes of zero stretching rate (L_1 and L_2) define the boundaries between (s) and (e) sectors. At the finite deformation state ($R_{XZ} = 5, 10$), the lines that bound the material line sectors correspond to L-axes of flow at the onset (L_{b1} and L_{b2}) and at the end (L_{a1} and L_{a2}) of deformation. (b) Schematic illustration of the analytical procedure employed to estimate W_m from a set of deformed veins (or dykes) in a cross-sectional outcrop face (i); after Passchier (1990b). (ii) The orientations of individual deformed veins are plotted on a diagram to determine the boundaries between veins with different stretch histories; (iii) the boundaries between (s), (e) and (se) sectors are then established taking into account the competence contrast between veins and matrix; (iv) the sectors are plotted in a Mohr circle (of arbitrary size) for tensor **H** and then tie lines are drawn to find the axes origin (v). The W_m is equal to the ratio Q/R.

increment of deformation. The notation L_{bi} and L_{ai} ($i = 1,2$) is used for these four lines where the subscripts 'b' and 'a' refer to 'before' and 'after' deformation (Passchier, 1990b). During progressive deformation with $W_m < 1$, both L_b lines as well as all material lines with intermediate orientations between these lines will extend as they rotate toward the apophysis A_2. All other rotated material lines, in turn, can be either shortened-then-extended or only shortened depending on if they did or did not pass, respectively, through the directions of L_i axes. Therefore, the L_{bi} lines always define the boundaries of the (e) sector, while the L_{ai} lines define the boundaries of the (s) sector (Fig. 7a). The arcuate sectors L_{a1} ^ L_{b1} and L_{a2} ^ L_{b2} contain material lines that have first been shortened-then-extended (se) and are interposed between the (s) and (e) sectors. During progressive simple shear, L_{b1} progressively rotates while the L_{b2} is fixed to shear plane and remains parallel to L_{a2}. Hence, the (e) and (s) sectors are separated by one (se) sector (Fig. 7a). Summarizing, for steady deformation with $W_m (=W_n) < 1$, the material lines sectors should be distributed on an orientation diagram as follows (Fig. 7a) (Passchier, 1990a,b):

L_{b1} – (e) – L_{b2} – (se) – L_{a2} – (s) – L_{a1} – (se) – L_{b1},

while for $W_m = 1$ this distribution is modified to (Fig. 7a):

L_{b1} – (e) – $L_{b2/a2}$ – (s) – L_{a1} – (se) – L_{b1},

These sectors distributions are valid for both non-dilatant and dilatant flows, and imply that the size of the (se) sector between L_{b2} and L_{a2} generally diminishes with increasing W_m values (Fig. 7a). Theoretically, an (es) sector can also be developed between L_{b2} and L_{a2} lines for $W_m > 1$ (Passchier, 1990b; Kuiper and Jiang, 2010), although in nature such stretch behaviour of material lines (i.e. folded boudins) is commonly the result of polyphase rather than a single phase of deformation (e.g. Passchier and Trouw, 2005).

The size of material line sectors depends not only on W_m but also on finite strain and A_n (Fig. 7a). For example, as is indicated by Eq. (10), the angle between L_{a1} ^ L_{a2} is a function of A_n. An easy way to obtain W_m values is by using the Mohr circle for the tensor **F** or its reverse **H,** although the analysis is commonly performed for **H** following the procedure summarized below (see Passchier, 1990b; Kuiper and Jiang, 2010 for details). In a Mohr diagram for **H** (Fig. 7b), the L_a lines are represented by the intersection points of the circle with a vertical axis. This axis passes through the circle centre if $A_n = 0$ and lies to the left or to the right of the centre if A_n value is negative or positive, respectively. Using these properties, all stretch sectors and *L*-lines of an orientation diagram, which represents the distribution of deformed veins on an outcrop surface (Fig. 7b:i–iii), can be plotted in a Mohr circle of arbitrary size, in such a way that the L_{a1}–L_{a2} axis is vertical (Fig. 7b: iv). As schematically illustrated in Fig. 7b: (v), tie lines are then drawn to find the origin of Mohr space. Thus, an estimation of W_m is obtained by measuring the ratio Q/R directly from the circle (Eq. (12); Fig. 7b: v). The scale of the Mohr diagram is also determined to calculate strain ratio (Passchier, 1990b).

The method represents a very good exercise for understanding the stretch history of material lines in a homogeneous deformed material. Moreover, the advantage of this method is that it relies on the orientations of lines, which in most cases can be fairly accurately measured. However, its application to naturally deformed rocks has some problems. The methods only work if the deformation has accumulated by approximately steady-state and homogeneous flow, on the scale of the analysed surface area (Passchier, 1990a,b). Also, the boundaries of sectors of folded, boudinaged and folded-then-boundinaged veins and dykes may not coincide precisely with to L_a and L_b lines (Fig. 7b: ii, iii) (Talbot, 1970; Ramsay and Huber, 1983; Passchier, 1990b). For example, if a high competence contrast occurs between vein material and matrix, veins may completely unfold when passing from the (s) to (e) field and consequently the folded-then-boundinaged sector will be narrower than the actual (se) sector. In the case of a low competence contrast veins absorb a certain amount of longitudinal shortening or extension after they pass an *L*-axis and before they begin to buckle or boudinage (Passchier, 1990b). Possibly, a correction for the orientation of L_a and L_b lines between material line sectors can be made if the competency contrast is known. Moreover, especially in general flows with area decrease, some (e) and (se) material line sectors become very narrow at relatively low strain values (Fig. 7a). It is doubtful if the boundaries between such sectors can be specified in practice.

4.2. Rigid porphyroclasts

Several studies (Ghosh and Ramberg, 1976; Passchier, 1987a; Simpson and De Paor, 1993; Masuda et al., 1995; Marques and Coelho, 2003) argued that the rotation of rigid porphyroclasts embedded in a ductilely deforming matrix depends on the vorticity of flow among others factors. The theoretical basis of these studies is Jeffrey's (1922) model that assumes: (a) particles are rigid ellipsoids; (b) particles are perfect bonded to the matrix; and (c) the matrix behaves as Newtonian linear-viscous fluid. For simple shear flow, this model predicts that all ellipsoidal particles rotate continuously and synthetically to the shear direction. For general shear neither are all rigid objects free to rotate continuously nor do all objects rotate synthetically to the shear direction (Fig. 8a) (Ghosh and Ramberg, 1976; Passchier, 1987a). In this case, the behaviour of clasts depends on their aspect ratio and initial orientation as well as on W_m. Thus, stable orientation analysis for a population of rigid porphyroclasts in a ductilely deformed rock can serve as a vorticity gauge (Passchier, 1987a; Masuda et al., 1995). In the current literature, analyses are commonly performed using two vorticity methods; the *porphyroclast aspect ratio* (PAR) method (Passchier, 1987a) and the *porphyroclast hyperbolic distribution* (PHD) method (Simpson and De Paor, 1993, 1997). Both methods and their variants have been applied in numerous studies (e.g. Wallis et al., 1993; Klepeis et al., 1999; Xypolias and Koukouvelas, 2001; Bailey and Eyster, 2003; Law et al., 2004; Jessup et al., 2006; Carosi et al., 2006; Johnson et al., 2009a; Langille et al., 2010; Thigpen et al., 2010a,b) for estimating W_m in natural ductile shear zones.

The PAR method (Passchier, 1987a) utilizes a population of tailed porphyroclasts with varying aspect ratios (R = long axis/short axis) and records graphically their rotational behaviour in the XZ plane by plotting a sectional clast shape factor, $B(=(R^2 - 1)/(R^2 + 1)$; Passchier, 1987a), against the angle, φ, between the long axis of clast and the flow plane (Fig. 8b). For high-strain rocks, the flow plane is considered to be parallel to the straight tails of porphyroclasts; although most published studies take the trace of macroscopic foliation as the reference frame. Theoretically, on such graphs two fields of behaviour for rotated clasts can be distinguished: (a) a field where the clasts with low shape factor and δ-type tails rotate infinitely and hence display a wide range in their long axis orientations; and (b) a field where the clasts rotate slowly (forward or backward) forming σ-type tails as they approach asymptotically a stable sink orientation (Fig. 8b). The critical shape factor B_c that behaves as a cut-off point separating these two fields defines the W_m:

$$W_m = B_c \quad (13)$$

Graphs for natural porphyroclast systems, however, often exhibit a gradual transition rather than an abrupt change between these two fields (e.g. Jessup et al., 2007). In such cases, the asymptotic curves, which define the theoretical predicted orientations of clasts

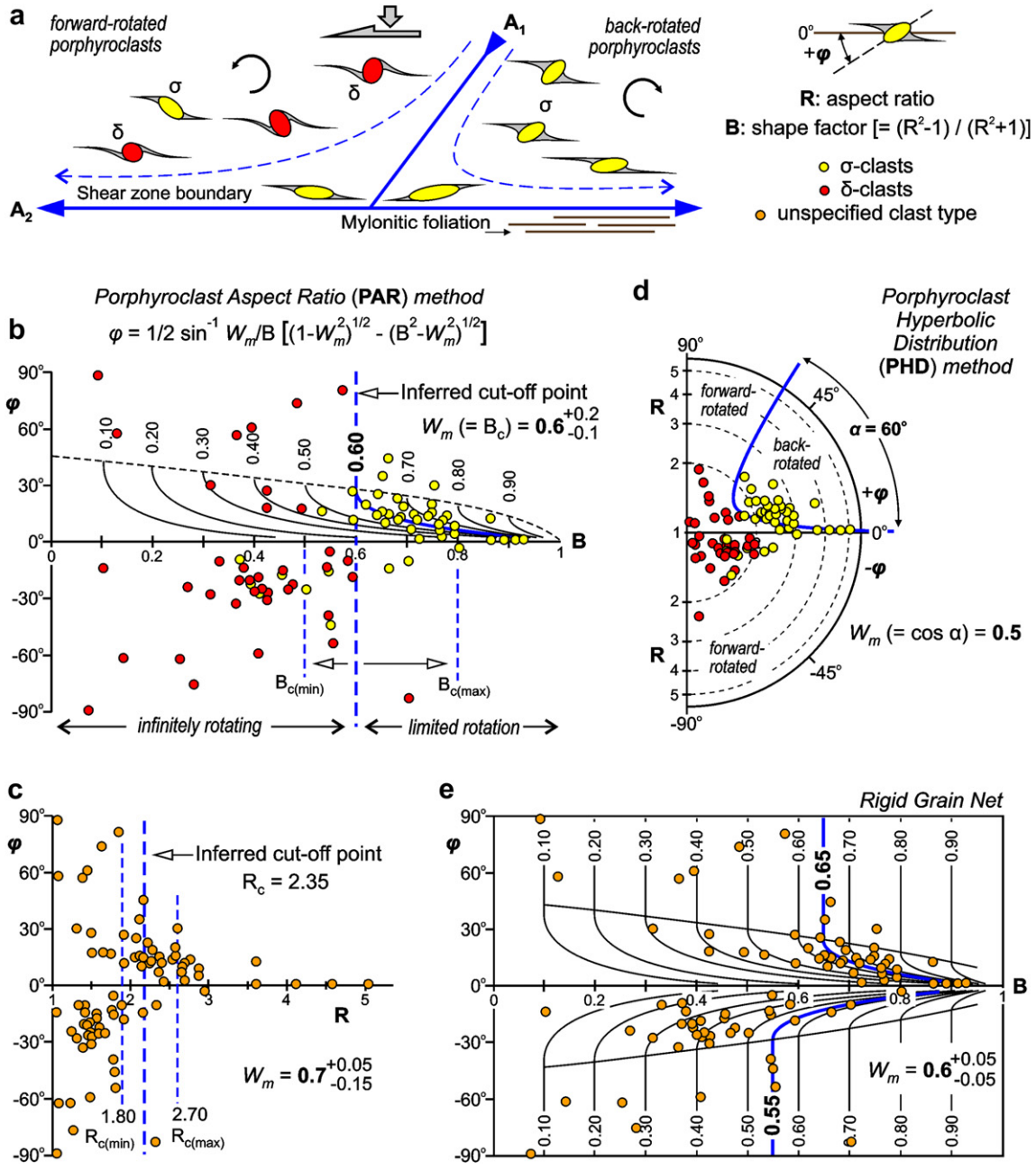

Fig. 8. Explanation and application of methods that use rigid porphyroclasts to estimate W_m; the yellow ornament corresponds to σ-porphyroclasts and the red to δ-porphyroclasts (a) Diagram showing the rotational behaviour of σ- and δ-type porphyroclasts in a sinistral general shear zone (modified after Simpson and De Paor, 1993; De Paor, 1994). (b) Orientation analysis of a population of tailed clasts using the porphyroclast aspect ratio (PAR) method (after Passchier, 1987a). The equation and its graphical presentation (asymptotic curves) define the theoretical predicted orientation of clasts at stable sink position at various W_m values. (c) Application of PAR method using an alternative and simpler graphical approach (after Wallis et al., 1993). Notice that all clasts are treated as tailless. (d) Orientation analysis of a population of tailed clasts using the porphyroclast hyperbolic distribution (PHD) method (after Simpson and De Paor, 1993). Hyperbola with interlimb angle 60° represents tightest hyperbola that separates back- from forward-rotated clasts (modified after Simpson and De Paor, 1997). (e) Orientation analysis of a population of clasts using the Rigid Grain Net (after Jessup et al., 2007); all clasts are treated as tailless. The two bold semi-hyperbolas delineate the potential range in W_m. All plots (b, c, d, e) were constructed using the same set of porphyroclast data (from Passchier, 1987a; his fig. 10). (For interpretation of the references to colour in this figure legend, the reader is referred to the web version of this article.)

at stable sink position for various W_m values (Fig. 8b; Passchier, 1987a), may help to specify the best B_c value, but a range of W_m values reflecting the uncertainty in evaluating B_c should be given. Wallis et al. (1993) followed an alternative graphical approach that simplifies the application of PAR method. Accordingly, all porphyroclasts are treated as tailless and a critical aspect ratio (R_c) is then specified by plotting the angle, φ, versus the aspect ratio, R, of porphyroclasts (Fig. 8c). Here, the W_m can be determined using the relation (Passchier, 1987a):

$$W_m = \left(R_c^2 - 1\right) \Big/ \left(R_c^2 + 1\right) \quad (14)$$

The PHD method also utilizes tailed porphyroclasts, and plots the aspect ratio (R) and the orientation (φ) of clasts in polar coordinates using the hyperbolic net (Fig. 8d; Simpson and De Paor, 1993, 1997). On this graph, backward rotated σ-type clasts and all other types of clasts define two, theoretically distinct, fields that can be separated by a hyperbola of the net (Fig. 8d). One limb of this hyperbola is selected to be asymptotic to the mylonitic foliation, assuming that it is

sub-parallel to the extensional flow apophysis, while the other is considered to delineate the orientation of the unstable flow apophysis. Thus, the cosine of the opening angle, α, of the chosen hyperbola gives the W_m (Eq. (8); Fig. 8d). Forte and Bailey (2007) emphasized that the angle, α, can also be obtained from a radial distribution plot using data from back-rotated clasts only. They investigated the accuracy of the PHD method and determined that the error inherent in W_m values ranges from ± 0.14 for end-member pure shear to ± 0.01 for end-member simple shear. Also, Yamaji (2008) proposed that the PHD method can be simplified by using the gnomonic net as an alternative means for estimating W_m and its uncertainty.

Recently, Jessup et al. (2007) compared and unified all above-described methods (Fig. 8b–d) proposing the *Rigid Grain Net* (RGN) as an alternative graphical technique for estimating W_m (Fig. 8e). In fact, the RGN is a modification of the original plot proposed by Passchier (1987a) and includes a series of semi-hyperbolas that are also mathematical equivalent to the hyperbolic net. The comparison showed that all methods (including RGN) generally yield internally consistent W_m values independently of whether they use tailless or tailed porphyroclasts (Fig. 8b–e). However, the PHD method tends to overestimate slightly the pure shear component.

The application of rigid porphyroclast methods, over the last ten years, has proved extremely useful for quantifying vorticity of flow in shear zones, but the accuracy of W_m estimates is affected by a number of factors. Several prerequisites must be met (e.g. Passchier, 1987a). (1) The rigid clasts should be embedded in a homogeneously deformed and preferentially very fine grained matrix; although coarse-grained matrix can also behaves as a continuum (Marques and Burlini, 2008). (2) The shape of clasts should not change with deformation due to recrystallization or fracturing and it should closely approach orthorhombic symmetry. (3) The sample should consist of a population of clasts with a range of aspect ratios. If the clast population lacks members with large aspect ratios, the methods will tend to underestimate W_m (Law et al., 2004). (4) The strain must be sufficiently large to allow clasts to reach a stable sink position; otherwise the methods tend to overestimate W_m (e.g. Bailey et al., 2004). The presence of well developed δ-type clasts is a significant indication that the analysed rock has experienced sufficient deformation (Ten Brink and Passchier, 1995). Plots with well defined cut-off points also imply that clasts have reached their stable orientation (Xypolias and Kokkalas, 2006). (5) The analysed profile should be orthogonal to the rotation axis of the porphyroclasts, otherwise the methods will underestimate W_m. However, this criterion is difficult to check. Iacopini et al. (2008) investigated this problem examining the vorticity value variation in sections oblique (5–45°) to the VPP and showed that a significant underestimation of vorticity values of the order of 0.15 occurs only when the W_m is in the range 0.4–0.8. This error value should be used to correct W_m in any case. (6) Clasts should not interact mechanically. (7) All rigid-clast methods are unreliable if significant strain partitioning at the clast interface occurs. This prerequisite is because, a clast/matrix interface lubrication markedly influences the stable clast orientations as indicated by analogue and numerical studies (Ceriani et al., 2003; Mulchrone, 2007; Johnson et al., 2009a,b and reference therein). Recently, Johnson et al. (2009a,b) modelled the behaviour of lubricated clasts embedded in a linear-viscous (Newtonian) matrix and showed that the cut-off point (B_c or R_c) between permanently rotating and stable clasts shifts toward smaller values underestimating W_m. Notice that clast lubrication compromises the vorticity gauge also for non-Newtonian rheology but further work is required to evaluate the effects of non-linear behaviour (Johnson et al., 2009b). In practice, a good fit of natural data to the theoretical curves, such as in Fig. 8b, implies that the rotational behaviour of clasts follows the linear-viscous model of Jeffery (1922), which assumes coupling between the clast and the matrix. Consequently, a thorough comparison between natural and theoretical clast distributions is required to evaluate whether or not a clast population has enjoyed lubrication. In this case, a large data set (more than 100 points) with an appropriate dispersion is needed to make a valid interpretation (Johnson et al., 2009a).

4.3. Porphyroblasts

The pattern of inclusion trails in porphyroblasts may provide information about the amount of syntectonic rotation of porphyroblasts, with respect to a reference frame (e.g. shear plane; matrix foliation) (Schoneveld, 1977; Passchier et al., 1992; Mancktelow and Visser, 1993; Williams and Jiang, 1999). Based on this observation, as well as on the analytical work of Ghosh and Ramberg (1976), various authors have used porphyroblast-rich fabrics to quantify the vorticity of flow (Vissers, 1987; Wallis, 1995; Beam and Fisher, 1999; Iacopini et al., 2008). Assuming steady-state monoclinic flow, Ghosh (1987) showed, for example, that the amount of rotation of rigid spherical objects (e.g. garnet porphyroblasts) embedded in a ductile matrix can be combined with independent strain estimates from the matrix to calculate W_n. Also, Holcombe and Little (2001) assumed that the internal foliation (S_i) of porphyroblasts was in the undeformed state parallel to the shear plane (Fig. 9a), as well as the orientation of S_i relative to the external matrix foliation in the deformed state reflecting true syntectonic rotation of porphyroblasts (Fig. 9b), and proposed a relatively simple graphical method for determining W_m. In this method, the S_i orientation of individual porphyroblasts plots as a function of the orientation of their long axes and a W_m value is estimated by comparing the obtained distribution with graphs that illustrate the theoretical pattern of distribution curves for a range of different aspect ratios at constant W_m and shear strain (γ) values (Fig. 9c).

Methods utilizing rotated porphyroblasts as vorticity gauges do not require intense deformation of the analysed sample but they are subject to the other prerequisites for the rigid-clast methods. Moreover, some authors (e.g. Bell and Johnson, 1989; Bell and Newman, 2006) argued that spiral-shaped inclusion trails can be developed from successively overprinting crenulations or transposed foliations without rotation of porphyroblasts with respect to a fixed kinematic reference frame, and thus put in doubt the reliability of these methods. However, the validity of this "non-rotational" model of porphyroblasts development is questioned by many authors and remains a matter of considerable debate (e.g. Fay et al., 2009; Bons et al., 2009; Johnson, 2009 and reference therein). Passchier and Trouw (2005; p. 218) summarized a number of criteria for evaluating whether porphyroblasts have rotated with respect to kinematic axes of bulk flow or not, which should be considered before using the shape of inclusion trails as a rotation gauge.

4.4. Quartz c-axis fabrics

Quartz-rich tectonites are often characterized by single- or crossed-girdle quartz *c*-axis fabrics, which exhibit asymmetry (or symmetry) with respect to the trace of foliation in the XZ plane (Law, 1990). The degree of asymmetry (obliquity) of the central girdle segment of such fabrics is controlled by W_m and the finite strain (Platt and Behrmann, 1986), because during any steady-state deformation with $0 \leq W_m \leq 1$, (1) the maximum principal axis of the strain ellipsoid rotates toward parallelism with the flow/shear plane (A_2) with increasing strain or remains parallel to it in pure shear (e.g. Ramsay, 1980; Passchier, 1997), while (2) the central segment of quartz *c*-axis fabrics, as indicated by Taylor–Bishop–Hill fabric modelling (e.g. Lister and Hobbs, 1980) and assumed by many

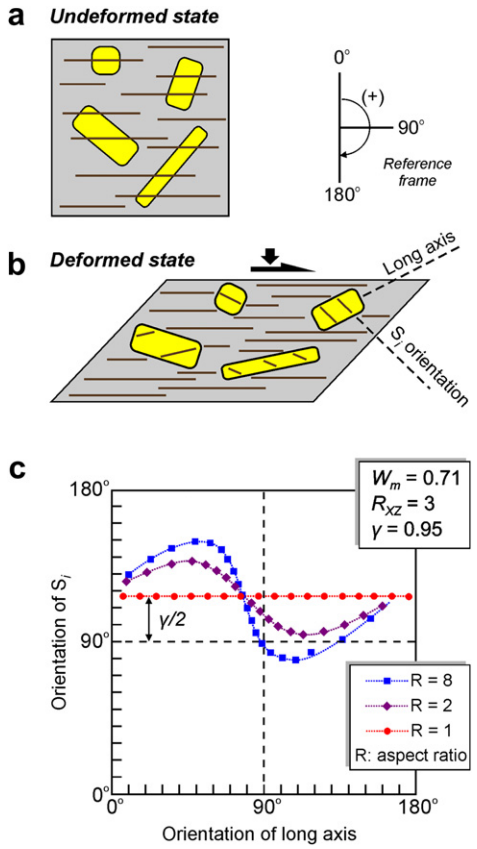

Fig. 9. Explanation and schematic illustration of the assumptions in the method used to estimate W_m from rotated porphyroblasts (modified after Holcombe and Little, 2001). (a) In the undeformed state, the initial orientation of internal foliation, S_i, in porphyroblasts is parallel to shear plane. (b) In the deformed state, the angular difference between S_i and the external foliation reflects true synkinematic rotation of porphyroblasts. Notice that all orientations angles (constrained to a 0–180° range) are measured in the sense of shear with the normal to the shear plane being 0°. (c) Theoretical predicted plot of the orientation of S_i versus the long axis orientation of individual porphyroblasts with different axial aspect ratios (R = 1, 3, 8) at constant W_m (= 0.71) and finite strain (R_{xz} = 3) values. Notice that the intersection of line containing equant objects (R = 1) with the S_i-axis is a function of shear strain (γ). In practice, plots of real data are analysed by comparison with theoretical plots produced by the software "GhoshFlow".

authors (Platt and Behrmann, 1986; Vissers, 1989; Wallis, 1992, 1995), establishes itself orthogonal to the flow plane (Fig. 10a: i). Based on this observation, Wallis (1992, 1995) showed that W_m can be calculated if both the strain ratio R_{XZ} and the angle β between the foliation and the perpendicular to the central girdle of a quartz *c*-axis diagram are known (Fig. 10a: i). The R_{XZ} data can be incorporated with β values either using the Mohr circle for tensor **F** (Wallis, 1992; see also Vissers, 1989) or by applying the following analytical solution:

$$W_m = \cos\left[\tan^{-1}\left(\frac{1 - R_{XZ}\tan^2\beta}{(1 + R_{XZ})\tan\beta}\right)\right] \quad (15)$$

that was recently proposed by the author (Xypolias, 2009) for simplifying the solution that had originally been derived by Wallis (1995; his eqs. (8) and (9)). Alternatively, estimates can be obtained graphically using the diagram of Fig. 10b, which shows the relationship between R_{XZ} and β for various W_m values.

This method (Wallis, 1995), which is known as *finite-strain/quartz c-axis-fabric* (R_{XZ}/β) method, has been widely used in studies of natural shear zones (e.g. Grasemann et al., 1999; Xypolias and Doutsos, 2000; Law et al., 2004; Sullivan, 2008; Sarkarinejad et al., 2010; Law, 2010; Xypolias et al., 2010). Such studies have identified potential sources of errors in the calculation of W_m. Specifically, as illustrated in Fig. 10b, W_m estimates using R_{XZ}/β method are very sensitive to small changes in the evaluated angle β (Grasemann et al., 1999; Law et al., 2004). Note that in the vast majority of published quartz *c*-axis-fabric diagrams, the angle β is determined with a minimum error of ±2°, because the central girdle segment is not perfectly straight (Fig. 10a: i) (e.g. Platt and Behrmann, 1986) and is commonly not well defined from the fabric data. Due to this uncertainty in determination of β, the method becomes unreliable in high-strain samples ($R_{XZ} > 15$) where the β is less than 5° for a wide range of possible W_m values (Fig. 10b) (Grasemann et al., 1999). Regarding the error in W_m values arising as a consequence of the uncertainty in estimating R_{XZ}, it is commonly overlapped by the error in W_m produced by the uncertainty in assigning β (Law, 2010; Xypolias et al., 2010).

Critical to the accuracy of W_m estimates is the central assumption that the quartz crystal fabrics remain in a stable orientation with respect to the external kinematic framework (Fig. 10a: i). This assumption is strongly supported by both experimental (e.g. for ice: Bouchez and Duval, 1982; for norcamphor: Herwegh and Handy, 1996) and numerical simulation studies (e.g. for quartz: Etchecopar and Vasseur, 1987; Jessell and Lister, 1990; Takeshita et al., 1999) as well as by observations in natural quartz mylonites (e.g. Burg, 1986; Law et al., 1990; Sullivan and Law, 2007). However, general shear experiments on quartz have produced fabrics whose central girdles develop oblique to the shear plane and rotate synthetically to shear direction with increasing strain and amount of dynamic recrystallization (e.g. Heilbronner and Tullis, 2006). In such cases, the R_{XZ}/β method tends to overestimate W_m (Law, 2010). These experimental findings seems to be in accordance with the petrofabric analysis of Law (2010 and references therein) from quartz mylonites in the Moine thrust zone (NW Scotland) where kinked single girdle quartz *c*-axis fabrics are clearly inclined to the thrust plane. Hence, the central assumption of the method should not be considered *a priori* valid for all natural occurring shear zones and, if possible, it should be independently checked by other criteria. For example, C-surfaces in C/S fabrics are thought to develop parallel to the shear zone boundaries (Fig. 10a) (Passchier and Trouw, 2005 and reference therein).

4.5. Macroscopic foliation

In monoclinic shear zones, the macroscopic foliation typically defines the XY principal plane of the finite strain ellipsoid. For volume-constant flow, its angular relationship (angle θ; Fig. 10a) with the shear zone boundary is unique for given R_{XZ} and W_m values (e.g. Fossen and Tikoff, 1993; Tikoff and Fossen, 1995). Thus, if θ and R_{XZ} are known, an estimate of W_m can be obtained (Wells, 2001; Bailey and Eyster, 2003; Bailey et al., 2004). This simple technique, usually called the R_{XZ}/θ-method, is equivalent to R_{XZ}/β method, and W_m is determined either using the diagram of Fig. 10b or applying Eq.(15) for $\theta = \beta$. Bailey et al. (2004) showed that θ can also be assigned from the angular difference between the foliation and C-shear bands provided that C-surfaces show small variability in their orientation. These authors have also argued that R_{XZ}/θ-method is valid for isovolumetric non-plane strain deformation and does not requires the assumption of steady-state deformation.

4.6. Oblique grain-shape foliation

Dynamically recrystallized aggregates of quartz and calcite often display within foliation-parallel domains of low- to medium-grade mylonites an oblique grain-shape fabric (Law et al., 1984, 1990; Lister and Snoke, 1984; Trullenque et al., 2006), which is interpreted to be

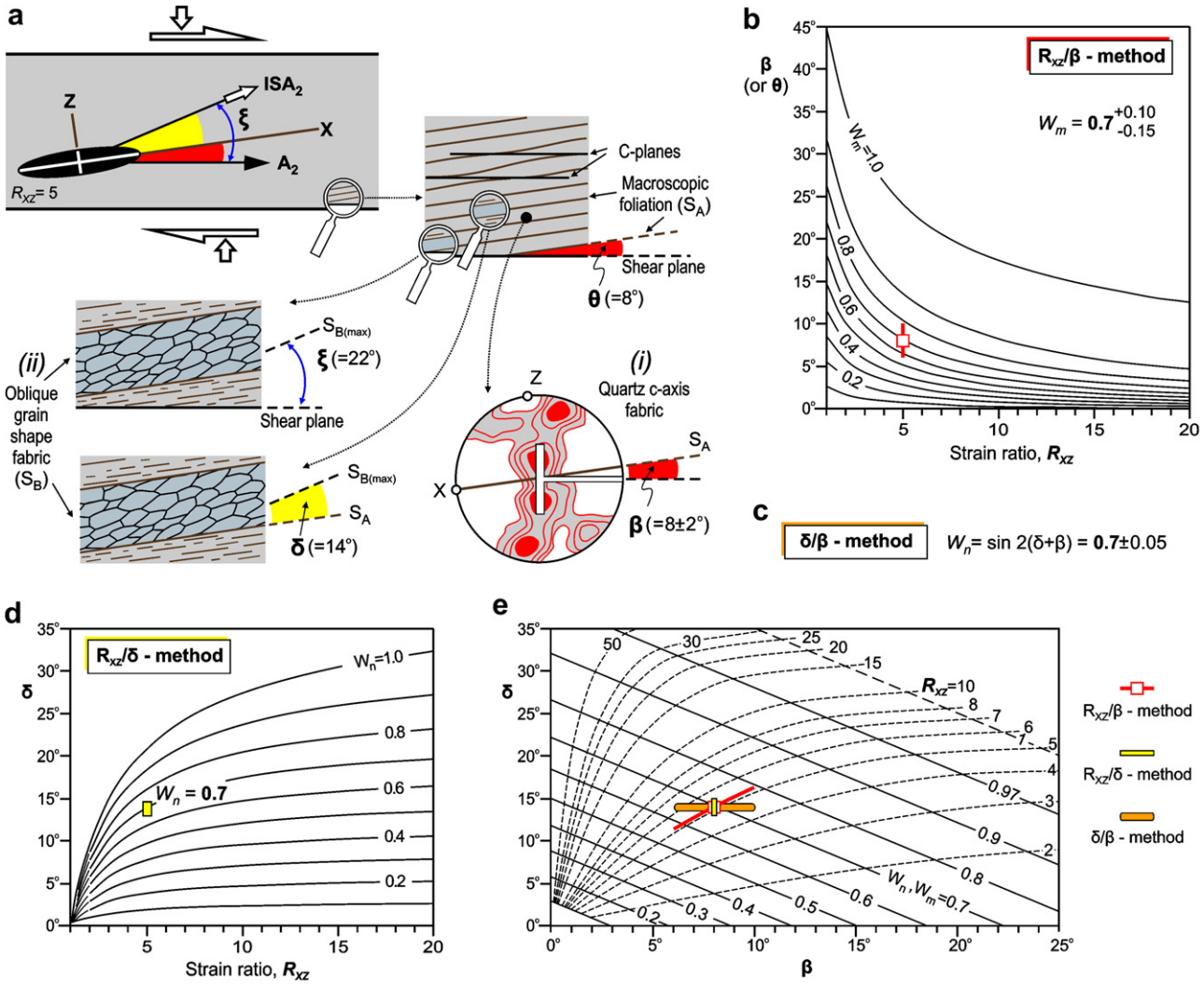

Fig. 10. Explanation and application of the R_{XZ}/β, R_{XZ}/δ and δ/β vorticity analysis methods for a hypothetical general shear zone. (a) Schematic illustration of the basic assumptions of methods. (i) The central girdle segment of quartz *c*-axis fabrics is oriented perpendicular to the shear/flow plane, A_2. (ii) The long axes of quartz neoblasts with an oblique grain-shape fabric nucleate parallel to the extensional ISA_2. (b) Plot showing the finite strain ratio R_{XZ} versus angle β (or θ) for various W_m values (after Tikoff and Fossen, 1995; Grasemann et al., 1999) and vorticity estimate for the hypothetical example. (c) Application of δ/β method. (d) Plot showing the finite strain ratio R_{XZ} versus angle δ for various W_n values (after Xypolias, 2009) and vorticity estimate for the hypothetical example. (e) Nomogram that incorporates all the parameters involved in the three vorticity methods (after Xypolias, 2009) and corresponding $W_{m,n}$ estimates for the hypothetical example.

the result of a complex process of continuous nucleation, passive deformation and rotation of the recrystallized grains (e.g. Means, 1981). According to Wallis (1995), the orientation of the long axes of quartz neoblasts within an oblique foliation delineates the direction of the extensional ISA_2 (Fig. 10a: ii). Supportive evidence for this assumption is given by experimental studies (Dell'Angelo and Tullis, 1989; Ree, 1991; Herwegh and Handy, 1998), which showed that such oblique grain-shape fabrics nucleate with their long axes in a fixed orientation with respect to the imposed kinematic reference frame of progressive deformation. Therefore, the greatest recorded angle between the oblique foliation and the shear zone boundaries should theoretically be equal to the angle ξ between ISA_2 and the flow apophysis A_2 (Fig. 10a: ii; Wallis, 1995). As a consequence, vorticity estimates can be obtained using the Eq. (9) (e.g. Daczko et al., 2001). Oblique grain-shape fabrics are instantaneous sensitive features and thus such estimates possibly record the W_n at the final increment of ductile deformation rather than W_m (Wallis, 1995).

In quartz-rich tectonites, the maximum recorded angle, δ, between the oblique and the main foliation in combination with the angle, β, between the shear/flow plane and main foliation determined from the quartz *c*-axis fabrics can also be used to assign ξ, if the shear zone boundary is unknown. Thus Eq. (9) can be rewritten as (Wallis, 1995):

$$W_n = \sin 2(\delta + \beta) \tag{16}$$

This simple and useful method is commonly referred to as *oblique-grain-shape/quartz c-axis-fabric* method or shorter δ/β-method (Fig. 10c) (Xypolias and Koukouvelas, 2001; Sullivan, 2008; Frassi et al., 2009; Law, 2010). Its drawback, however, is that it is based on two major hypotheses: one regarding the orientation of ISA_2, and one regarding the orientation of flow plane. Despite that fact, W_n estimates using δ/β-method are not sensitive to small uncertainties in β values. The uncertainty in assigning δ has not been investigated so far but is not expected to be great. However, frequency distribution graphs used to determine δ often exhibit continuous populations of orientation data and single outliers with large values (e.g. Frassi et al., 2009; their fig. 9b; see also Knipe and Law, 1987; their figs. 1, 2 and 8). In such cases, the angle δ may be assigned from the maximum value of continuous population of

readings (Frassi et al., 2009; Xypolias et al., 2010). Alternatively, Johnson et al. (2009a) addressed this problem by applying a statistical approach for a suite of samples. In this case, an average W_m value is obtained by adding an appropriate average correction for the β angle to measurements of δ in each sample.

Experiments in polycrystalline norcamphor by Herwegh and Handy (1998) have also revealed that the value of angle δ is closely related to the vorticity of flow as well as to the shape of the strain ellipse just before the end of deformation. Xypolias (2009) used this finding to show that for a given pair of (R_{XZ}, δ) values, the W_n can be calculated by applying the equation:

$$W_n = \sin(2\delta)\frac{R_{XZ}+1}{R_{XZ}-1} \quad (17)$$

Plot of R_{XZ} versus δ for various W_n values (Fig. 10d) indicates that W_n-curves increase spacing with increasing strain values and therefore, vorticity estimates from this method (called as R_{XZ}/δ − method) are relatively insensitive to small changes in values of input parameters. However, the method is more appropriate for rocks that record R_{XZ} values greater than ca. 4–5 (Xypolias, 2009).

Moreover, application of both aforementioned methods (δ/β, R_{XZ}/δ) as well as of R_{XZ}/β method can also be performed utilizing the vorticity nomogram illustrated in Fig. 10e. This graph incorporates all the parameters (δ, β, R_{XZ}) involved in quartz-based vorticity analysis and allows the investigator to check, for all methods, the sensitivity of estimated vorticity values to changes of these parameters. It also provides a rapid means for evaluating the consistency of vorticity estimates obtained by all three methods.

4.7. Shear bands − flanking structures

C′-type shear bands represent one of the most frequent structures in general shear zones (Platt and Vissers, 1980; Behrmann, 1987; Grasemann and Stüwe, 2001) and may serve as another potential means for estimating vorticity of flow. Yet, the geometric relationships between shear bands and the elements of flow are not fully understood. For example, some authors (Bobyarchick, 1986; Pray et al., 1997) have suggested that shear bands synthetic to the far-field shearing may nucleate parallel to the inclined flow apophysis A_1. Others (Platt and Vissers, 1980; Simpson and De Paor, 1993) have proposed a possible association of shear bands with the directions of minimum and maximum angular velocities of material lines in general flow (Ω_1 and Ω_2 in Fig. 5), which implies that synthetic and antithetic shear bands nucleate parallel to the acute and obtuse bisector of the flow apophyses, respectively, and progressively rotate toward the shear/flow plane, A_2 (Fig. 11). Convincing supporting evidence for the latter hypothesis was recently provided by Kurz and Northrup (2008) from natural mylonitic rocks, who evaluated the angle α between the A_1 and A_2 using the PHD method and then recognized: (1) that the synthetic shear bands in the analysed rocks are oriented either parallel to, or at an angle less than the acute bisector, and (2) that the antithetic shear bands are poorly-developed and have a mean inclination parallel to the obtuse bisector of the flow apophyses (Fig. 11). These findings are in good agreement with the model proposed by Platt and Vissers (1980) for non-coaxial deformation according to which the synthetic shear bands rotate very slowly toward the flow plane remaining active longer than high-angle antithetic shear bands that rotate rapidly and become inactive. Hence, the largest recorded angle between the synthetic C′-type shear bands and the shear plane is equal to half of angle α, and consequently an estimation of W_m is obtained by using Eq. (8) (Fig. 11) (e.g. Kurz and Northrup, 2008; Sullivan, 2009).

The rotational behaviour of shear bands during progressive deformation has also been investigated in the frame of numerical

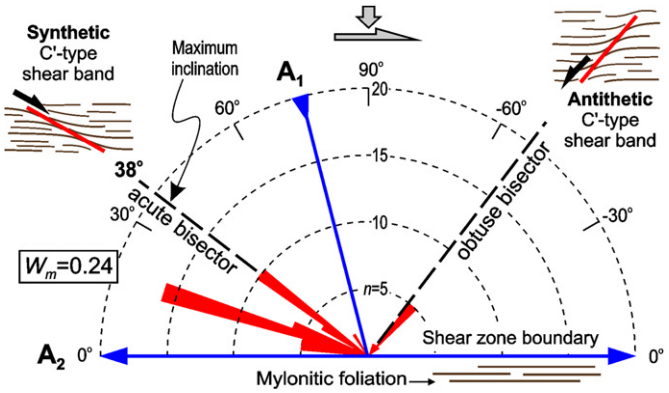

Fig. 11. Rose diagram showing orientations of synthetic and antithetic C′-type shear bands (data after Kurz and Northrup, 2008); n: number of measurements. Twice the greatest angle (2 × 38°) between the synthetic shear bands and the shear zone boundary (defined by the mylonitic foliation) is considered to be approximately equal to the angle between the apophyses A_1 and A_2, and hence $W_m = 0.24$ (=cos76°; Eq. (8)).

models for the instantaneous development of flanking structures/folds (Fig. 12a: 1–10; e.g. Grasemann et al., 2003). Typical synthetic C′-type shear bands (Fig. 12a: 8–10) are an example group of flanking structures (see Passchier, 2001; Grasemann and Stüwe, 2001; Grasemann et al., 2003; Wiesmayr and Grasemann, 2005; Coelho et al., 2005 for details). Such numerical studies have shown that normal shear bands with a stable (i.e. non-rotating) and shallowly inclined orientation (<30°), with respect to the flow plane, are characteristic of general flows with W_n around 0.6–0.8 (α = 40–50°) (Fig. 12a: 9). Normal-sense shear bands can also develop in all other flow types but in those cases are unstable and, in some cases, can evolve to other flanking structures. These results seem to be in accordance with natural observations, which argue that C′-type shear bands typically form at an angle of 15–35° with respect to the boundaries of shear zones (e.g. Berthé et al., 1979; Platt and Vissers, 1980). The model also predicts that conjugate sets of shear bands are more likely to be observed in pure shear dominated flows with W_n less than 0.6 (Grasemann et al., 2003). Therefore, these results can be used to determine the possible range of values of vorticity number in naturally deformed rocks (e.g. Xypolias et al., 2010).

Nevertheless, this model (Grasemann et al., 2003) does not use the hypothesis that normal shear bands develop parallel to the acute bisector of the flow apophyses and progressively rotate toward the flow plane. The normal shear bands are assumed to result from back- or forward- or non-rotation of any isolated planar element that dips less than the inclined apophysis A_1 and transects the foliation at an instant during the progressive mylonitization of rock. Such a forward- or non-rotation of a gently inclined cross-cutting element (Fig. 12a: 8a and 9) is in contrast, however, with the rotational behaviour of passive markers in general flows and may not be possible in anisotropic rocks (e.g. Kocher and Mancktelow, 2006). From the above discussion, vorticity estimates based on normal-sense shear bands should be considered with caution.

Grasemann et al. (2003) have also shown that nearly all flanking structures are unstable and that they can evolve from one type to another during progressive deformation (Fig. 12a) where stable normal-sense shear bands are the exception. The type of resultant structure at the end of deformation depends on the vorticity of flow and the finite strain as well as the initial orientation of the cross-cutting element. Realizing this, Gomez-Rivas et al. (2007) proposed a graphical method for estimating W_m from a population of flanking structures embedded in mylonitic rocks assuming that the cross-cutting elements of structures behave as passive markers in

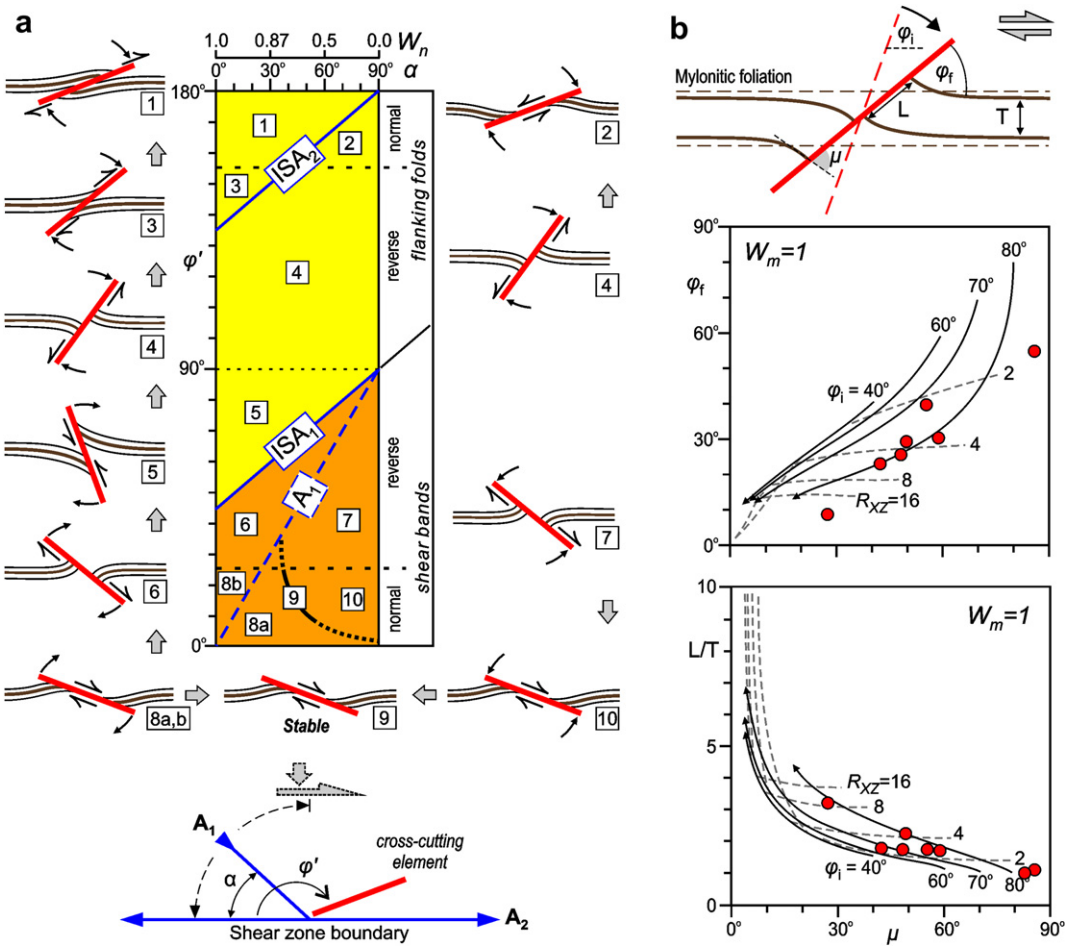

Fig. 12. (a) Diagram summarizing the results of numerical models for instantaneous flanking structures (1–10) development as a function of W_n and initial orientation, φ', of cross-cutting element in dextral shear zones (after Grasemann et al., 2003; Wiesmayr and Grasemann, 2005). According to the model, natural normal-sense (C′-type) shear bands (9) are only stable in a general flow with W_n around 0.6–0.8. (b) Geometric parameters and graphs required for applying the flanking structure method of vorticity analysis proposed by Gomez-Rivas et al. (2007); φ_i: initial orientation of the slip surface with respect to mylonitic foliation; φ_f: the final orientation of the slip surface; μ: maximum drag angle between the foliation and the slip surface; L: thickness of a deflected foliation-parallel marker layer at the slip surface; and T: thickness of marker layer further away from the slip surface. The points on the graphs follow the theoretical curves for $W_n = 1$ and initial orientation of 70–80° (data after Gomez-Rivas et al., 2007; their fig. 5).

a viscous medium. The method requires measurements of a number of simple parameters describing the geometry of individual structures on planes perpendicular to the foliation and the slip surface and details of the procedure are summarized in Fig. 12b. The vorticity is determined by plotting the measurements on a series of graphs with theoretical curves, which show the expected progressive variation of measured parameters with increasing strain at constant W_m and given initial orientation of the cross-cutting elements. The key assumption of the method is that the analysed flanking structures nucleate at different stages during progressive steady-state deformation, but all at approximately the same orientation. Moreover, the slip surface of structures should be sharp and discrete, and for this reason normal shear bands are not suitable for this method (Gomez-Rivas et al., 2007).

4.8. Tension gashes and tectonic stylolites

Arrays of tension gashes are common features of brittle–ductile shear zones (Ramsay, 1980) and their formation is thought to be controlled by several factors including vorticity (e.g. Smith and Durney, 1992). It is commonly assumed that tension gashes nucleate as opening fractures orienting parallel to the shortening ISA_1 (Fig. 13). During progressive non-coaxial deformation, the central portion of the gash vein rotates synthetically to shear direction as it widens but the fracture will continue to propagate outward in the direction of ISA_1. Also, tension gash veins are occasionally accompanied by the development of fibres or elongate grains in vein material. In non-coaxial deformation, new fibre segments are grown parallel to the extensional ISA_2 while older ones are rotating out of this direction (Ramsay and Huber, 1983). Therefore, if the orientation of fracture tips and/or the orientation of newly-grown fibres of tension gash veins, with respect to the shear zone boundary, is known, the vorticity number can be estimated using Eq. (9) (Fig. 13) (Fossen and Tikoff, 1993; Tikoff and Fossen, 1995). These structures are time sensitive and thus they provide information for W_n. Grasemann et al. (1999) have used such tension gashes to estimate vorticities related to the later stages of deformation of the Greater Himalayan Series in the NW Indian Himalaya that post-date the dominant penetrative deformation associated with mountain building.

Veins formation is largely synchronous with pressure solution phenomena and therefore the direction of shortening ISA_1 can be independently evaluated by stylolites and slickolites since their teeth are oriented parallel to this direction (Fig. 13) (e.g. Ebner et al., 2009 and references therein). Ebner and Grasemann (2006) showed that the angle of obliquity of slickolite teeth may be used to estimate W_n at the latest deformation increment of a ductile high-strain zone, if it can be proved that the post-mylonitic

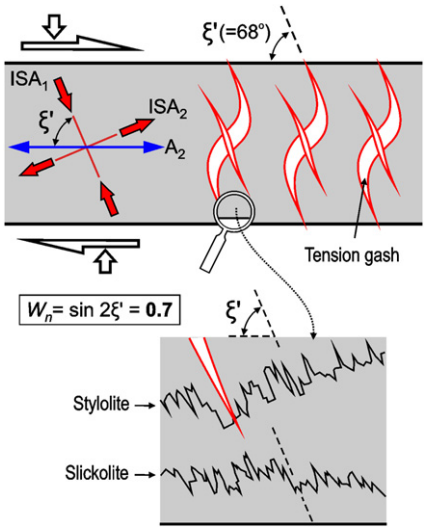

Fig. 13. Hypothetical general shear zone with tension gash veins and pressure solution features (stylolites, slickolites), from which W_n can be determined. Fracture tips of tension gashes (cf. Grasemann et al., 1999) as well as stylolites and slickolites teeth are oriented parallel to the shortening ISA_1.

pressure solution deformation is localized on surfaces parallel to the mylonitic foliation. In this case, an estimation of A_n is also obtained assuming zero elongation parallel to the flow plane.

4.9. Other vorticity gauges

Several other microstructures can also be used as potential means for extracting W_m from rocks. Tikoff and Teyssier (1994) used the interaction of porphyroclasts as a vorticity gauge and demonstrated that the proportion of imbicated clasts increases with increasing finite strain and with increasing pure shear component. Therefore, if finite strain and number of imbricated clasts are known, an estimate of W_m can be obtained. Mulchrone et al. (2005) modelled the behaviour of tiled phenocrystal pairs in magmatic flow and showed that the proportion of tiled pairs, which are consistent with the sense of shear, decrease from 70% for simple shear to approximately 50% for flows approaching pure shear. According to this model, the tiling proportion can gives a reliable W_m value for the magmatic state of an igneous rock only if it is extracted from a sufficient number (at least 200) of observations. Giorgis and Tikoff (2004) numerically investigated the rotational behaviour of a population of oblate porphyroclasts in a viscous deforming Newtonian medium and showed that data for shape factor and the degree of anisotropy of the fabric ellipsoids can be combined to constrain the vorticity of a shear zone.

Experimental and computer simulation studies (e.g. Wenk et al., 1987) for the evolution of crystallographic preferred orientation of calcite in the twinning regime have yielded textures with *c* [0001]-axis point maximum oblique to the shear plane that rotate antithetically toward the shear direction with increasing simple shear component. Therefore, the angle of asymmetry of calcite *c*-axis fabrics can be used to determine W_m in calcite marbles (Wenk et al., 1987; Ratschbacher et al., 1991). However, the validity of this finding for calcite mylonites is strongly questioned by recent studies (e.g. Trullenque et al., 2006; Oesterling et al., 2007), which have demonstrated that *c*-axis point maximum rotate synthetically to the sense of shear if dynamic recrystallization during deformation is dominant compared to twinning.

5. Comparison of methods

Theoretically all of these vorticity gauges could be used to quantify vorticity of flow in an exhuming shear zone that formed in the ductile regime and remained active under brittle–ductile to brittle conditions. In this case, vorticity gauges will record different parts of the deformation history of the shear zone due to sequential development of structures at different conditions. Deformed sets of veins, rigid porphyroclasts/blasts, quartz *c*-axis fabrics and oblique grain-shape foliation should provide information for the mylonitic stage of deformation. C′-type shear bands possibly record the late syn-mylonitic or the early post-mylonitic deformation, inasmuch as it seems that they are generated at a late stage of shear zone activity when the mylonitic foliation is already established (e.g. Passchier and Trouw, 2005; pp. 128–132). The same is likely the case for flanking structures, in general. Arrays of tension gashes often occur early in the history of a brittle–ductile shear zone (Knipe and White, 1979) or at the end of the ductile deformation history of an exhuming shear zone (e.g. Grasemann et al., 1999), and therefore they should mainly describe the post-mylonitic stage.

In such a hypothetical shear zone, the application of all available vorticity methods will yield similar results only if the flow remained steady throughout the strain history, and the prerequisites of all the methods are met. Beyond this extreme example, steadiness of deformation in a ductile shear zone can be tested by applying individual methods, such as R_{XZ}/β and R_{XZ}/θ methods, in a suite of differently strained samples. If the deformation in the shear zone has accumulated by approximately steady-state flow, the estimates should plot along a specific W_m curve (e.g. Fig. 10b; Tikoff and Fossen, 1995). Also, steady-state conditions could be indicated if the application of all the quartz-based methods (R_{XZ}/β, R_{XZ}/δ and δ/β) in the same sample yields W_m estimates that plot to the same point on the vorticity nomogram (Fig. 10e; Xypolias, 2009).

5.1. The strain memory of methods for a non-steady flow history

Many vorticity studies in naturally occurring shear zones have shown that deformation is generally non-steady. In such cases, it is thought that most of the vorticity methods determine the mean value of flow vorticity, W_m, for the deformation stage of interest (e.g. mylonitic, post-mylonitic stage) while methods, which are based on instantaneous sensitive markers such as oblique grain-shape foliations, tend to record W_n just before the fossilization of the fabric. However, the vorticity methods used for determining W_m may have different degrees of sensitivity to changes in the flow regime. This difference implies that some methods likely record discrete parts of the deformation history, and hence may not provide meaningful estimates of mean vorticity. In fact, the relative length of "strain memory" of each method is not well understood, especially for those analysing the ductile stage of deformation. Generally, it is thought that deformation of pre-existing veins accesses a significant part of deformation history since they predate deformation (Passchier, 1990b). Probably the R_{XZ}/θ and the porphyroblasts methods also record a large part of the ductile deformation history inasmuch as they add rotational increments during the deformation (e.g. Passchier, 1988b). Similar problems exist with interpretation of the most widely used vorticity methods that utilize rigid porphyroclasts (e.g. PAR and PHD methods) and quartz *c*-axis fabrics (R_{XZ}/β *method*) (e.g. Law et al., 2004).

Some authors (Simpson and De Paor, 1997; Bailey at al., 2004; Sullivan, 2008) consider that rotating porphyroclasts are likely to equilibrate relatively quickly to vorticity changes, and therefore they do not provide reliable estimates of W_m because they record the vorticity at the waning stage of ductile deformation. In contrast,

other studies (e.g. Xypolias, 2009; Law, 2010) have suggested that the analysis of rigid porphyroclasts gives results close to the real mean vorticity of flow. A potential solution to this controversial issue could be given by comparing vorticity estimates of rigid grain methods with W_m or W_n values obtained by other methods. In the Hellenides of Greece, for example, Kumerics et al. (2005) reported vorticity numbers in the range 0.25–0.8 using rigid clasts (PAR method), which are consistent with W_m values of 0.15–0.7 obtained by deformed sets of veins in the same rocks. In the same orogenic belt, Xypolias (2009) reported vorticity estimates of 0.75–0.85 using rigid clasts (PAR method) and 0.85–1.00 using the R_{XZ}/δ method in samples from the same part of a shear zone. Taking into account that the R_{XZ}/δ method reflects the latest increments of plastic deformation of quartz, it seems that the results of PAR method remain unaffected by late-stage changes in the flow regime. A similar evaluation is made by comparing vorticity results reported by Bailey and Eyster (2003) from mylonitic rocks in the Pinaleno Mountain range (Arizona, USA). Here, vorticity analysis of ultramylonites using rigid clasts (PHD method) has yielded vorticity values of 0.1–0.3, while analysis of protomylonites using the R_{XZ}/θ method has yielded W_m estimates of 0.6–0.9. Therefore, rigid-clasts analysis records a pure shear dominated deformation in rocks (ultramylonites) that began to deform early in the history of the shear zone and appears to be unaffected by the increasing simple shear component recorded by the R_{XZ}/θ analysis of rocks (protomylonites) that started to deform later in the strain history (Bailey and Eyster, 2003). Also, in the northern Sardinian Variscides, Iacopini et al. (2008) obtained similar vorticity estimates ($W_m = 0.35 \pm 0.25$) from samples analysed using both the rigid-clast and the porphyroblast methods. Although these examples do not give a definitive solution to the problem, they support the view that rigid-clast analysis yields vorticity estimates close to W_m.

Questions often arise whether the R_{XZ}/β method, which utilize data from quartz *c*-axis fabrics, records a significant part of deformation history providing reliable estimates of W_m or whether it reflects only the last increments of ductile deformation. In trying to find solutions to such problems, many authors (e.g. Sullivan, 2008; Larson and Godin, 2009; Xypolias, 2009) correlate directly the length of strain memory of R_{XZ}/β method with the sensitivity of quartz *c*-axis fabrics to respond to temporal changes in flow regime. But can these two really be interrelated? An answer to this question can be given if we consider that the central hypothesis of the R_{XZ}/β method is valid; the central girdle segment of quartz *c*-axis fabrics establishes itself orthogonal to flow/shear plane independently from the flow type, which has been numerically modelled for plane strain under strict pure and simple shear conditions by Lister and Hobbs (1980). So, assuming that the quartz *c*-axis fabrics are very sensitive to flow changes, the finite crystallographic pattern will represent a reliable *qualitative* indicator of flow regime just prior to fossilization of the fabric. However, the central segment of such a fabric will be oriented perpendicular to flow plane as also occurred at the early increments of deformation. The central segment of the crystal fabric will retain the same orientation throughout the deformation history even assuming that the crystallographic fabric pattern equilibrates slowly to vorticity changes, as is possibly the case. This retention demonstrates that the degree of re-equilibration of the crystal fabric does not affect the critical angle β between the perpendicular to the central girdle segment of fabric and the foliation. In other words, the length of strain memory of the R_{XZ}/β method depends only on the orientation of foliation and consequently it is similar to that of R_{XZ}/θ method. Therefore, theoretically, both R_{XZ}/β and R_{XZ}/θ methods should always provide consistent estimates of W_m. Currently, only limited data are available to compare these two methods. Bailey et al. (2007) reported W_m estimates of 0–0.3 using R_{XZ}/β method and 0.2–0.6 using R_{XZ}/θ from a shear zone with the central Appalachian Blue Ridge, which generally support the above statements since both methods reveal pure shear dominated deformation.

5.2. Rigid-clasts method versus R_{XZ}/β method

From the above discussion, it follows that both the rigid-clast and R_{XZ}/β methods probably record a large portion of the ductile deformation history of a shear zone and consequently they should provide consistent results or at least significantly overlapping ranges of W_m values. But is that really so? Fig. 14 presents results obtained by various studies that have applied both vorticity methods to individual samples. The comparison reveals that in 70% of cases (17 out of 24 samples) these two methods give different estimates of W_m, while in the remaining cases a partial overlap of estimated values occurs and is considered to be

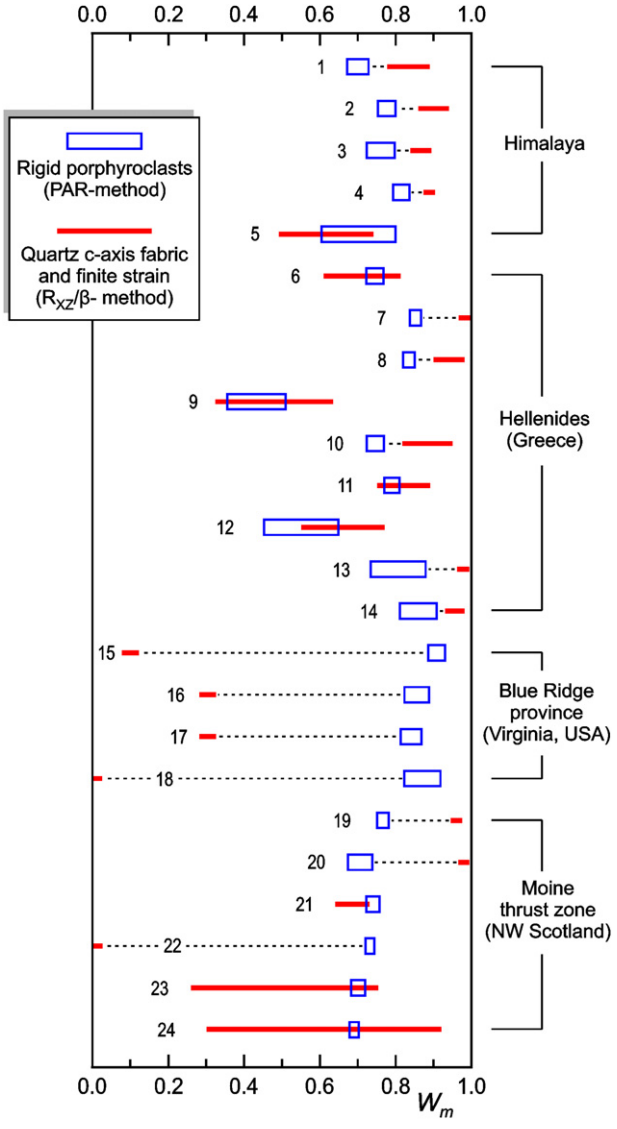

Fig. 14. Comparative diagram showing the range of W_m values obtained by applying both rigid porphyroclast and R_{XZ}/β methods of vorticity analysis to individual samples (1–24). Length of bars reflects the uncertainty in the calculation of W_m values. See text for discussion. Data for samples 1–4 after Law et al. (2004); 5 after Larson and Godin (2009); 6–11 after Xypolias and Kokkalas (2006); 12–14 after Xypolias et al. (2010); 15–18 after Bailey et al. (2007); 19–24 after Law (2010). Raw data are given as Supplementary information.

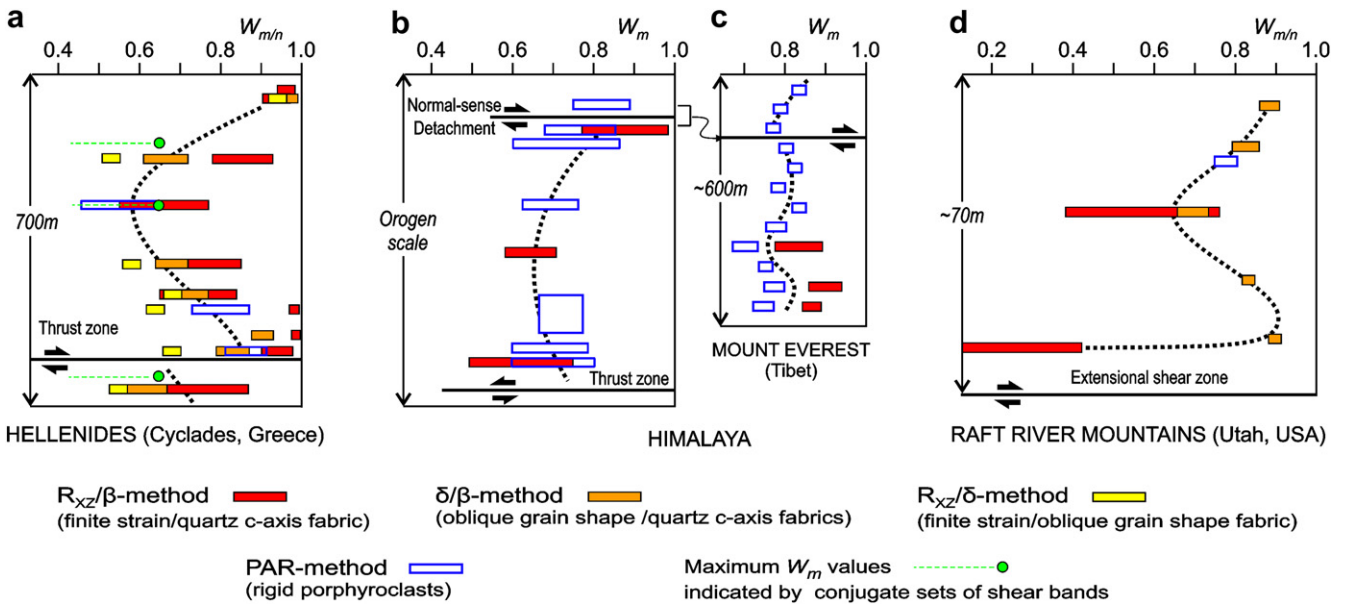

Fig. 15. Typical vorticity profiles across deformation zones in (a) Cycladic Blueschist belt (after Xypolias et al., 2010), (b) Greater Himalayan Slab in the Annupurna region of the Central Himalaya (after Larson and Godin, 2009 and references therein), (c) footwall to the South Tibetan detachment system in the Mount Everest area of the eastern Himalaya (after Law et al., 2004; Jessup et al., 2006) and (d) Raft River Mountains (after Sullivan, 2008). Length of bars reflects the uncertainty in the calculation of W_m (or W_n) values.

comparable. It is remarkable that in half of the samples, the W_m values obtained using rigid-clasts method are lower than values determined by R_{XZ}/β method (Fig. 14). This fact has been extensively discussed by Johnson et al. (2009a,b) who ascribed this discrepancy to the systematic underestimation of the rigid clast-based W_m estimates due to lubrication that often occurs at the matrix/clast interface. However, the effect of clast lubrication seems to be important only for flow with $W_m < 0.9$. An equally plausible explanation could also be that the R_{XZ}/β method overestimates W_m values if the central girdle segment of the quartz *c*-axis fabric rotates synthetically to the shear direction with progressive shearing (Law, 2010; Section 4.2). Another explanation discussed by Johnson et al. (2009a) is that if quartz is markedly weaker than the surrounding matrix, W_m values obtained by quartz-based methods could be anomalously high due to partitioning of shear strain and vorticity into quartz pools. Moreover, the comparison shows that in some samples, which mainly come from the same shear zone (Blue Ridge province; Bailey et al., 2007), the rigid-clasts method provides much larger W_m values than the R_{XZ}/β method (Fig. 14). Possibly, the primary cause of this difference is the relatively low strain in the zone that may lead to the overestimation of rigid clasts W_m estimates (Bailey et al., 2007). Therefore, it seems that a potential discrepancy between these two vorticity gauges could be due to a number of reasons such as the analytical problems of methods, the validity of adopted assumptions and the partitioning of flow at the sample scale (Law et al., 2004; Johnson et al., 2009a). As pointed out by Law et al. (2004), at the present state of knowledge, it is very hard to discriminate between these possibilities.

5.3. Reconstruction of spatial and temporal variation of vorticity

Even with these uncertainties, the application of as many vorticity methods as possible in a number of individual samples has proved extremely useful in evaluating the temporal (e.g. Wallis, 1995; Grasemann et al., 1999) and spatial (e.g. Xypolias and Koukouvelas, 2001; Law et al., 2004) variation of vorticity of flow within shear zones. Specifically, information about flow path can be retrieved by comparing estimates determined using methods that access different parts of the strain history of a shear zone (Passchier, 1988b). For example, Grasemann et al. (1999, 2003) reported W_m estimates of ca. 0.9 using quartz *c*-axis fabrics (R_{XZ}/β method), 0.6–0.8 using normal-sense shear bands and 0.55–0.7 using rotated tension gashes from mylonites of the Main Central Thrust zone (NW Himalaya). These results imply that the deformation history of the mylonitic zone commenced close to simple shear but progressively changed to a more pure shear dominated flow toward the last stages of brittle–ductile deformation (Grasemann et al., 1999) manifesting a *decelerating flow path* (Simpson and De Paor, 1993; Fossen and Tikoff, 1997). In the Sanbagawa belt (SW Japan), Wallis (1992, 1995) reported W_m values of 0.5–0.7 and 0.35–0.6 using deformed sets of veins and the R_{XZ}/β method, respectively, as well as W_n estimates of 0.7–0.8 using the δ/β method. These results indicate an increase in simple shearing during the final increment of ductile deformation implying an *accelerating flow path*. In the External Hellenides (Greece), Xypolias (2009) used vorticity values derived from rigid clasts and all available quartz-based methods to reconstruct the spatio-temporal variation of vorticity in a crustal scale shear zone, and distinguished sequential and zone-parallel domains that follow either a decelerating or an accelerating flow path.

Possibly in most shear zones the W_n varies in both space and time. Fig. 15 illustrates some indicative vorticity profiles across deformation zones of various scales. Although, such profiles are not always easy to interpret in terms of W_n history they enable us to discriminate, for instance, pure shear from simple shear dominated domains. Such information has considerable kinematic consequence since, for example, the increase in pure shear component of deformation toward the middle of the zone (Fig. 15a and b), especially when it is accompanied by a decelerating flow path, seems to be indicative for shear zones of ductile extrusion. Moreover, the deviation from simple shear along the shear zone boundary (Fig. 15a,c and d) indicates the presence of a stretching fault (in the sense of Means, 1989). Vorticity values can also be incorporated with finite strain data to evaluate the transport-parallel elongation and/or thinning in a zone (Wallis, 1995; Xypolias and Koukouvelas, 2001; Law et al., 2004; Xypolias et al., 2010; Law, 2010). In such cases, special attention is needed to avoid propagation of uncertainties involved in vorticity values.

6. Concluding remarks and perspectives

Quantitative analysis of flow vorticity in rocks can be performed with a wide range of methods that utilize a variety of geological structures and fabrics, including deformed sets of veins or dykes, porphyroclasts/blasts, crystallographic fabrics, oblique grain-shape fabrics, shear bands, flanking folds and tension gashes. However, all available methods of vorticity analysis rely on analytical models of homogeneous steady-state flows and are limited by a number of additional, but necessary, assumptions which are not always easy to verify in practice. Therefore, by definition, none of the methods can be considered as fully reliable although they remain the best tools we currently have available to extract vorticity numbers from naturally deformed rocks. Of course, a strict criticism could be that, at the current stage of method development, it is inappropriate to attempt to quantify flow vorticities in rocks when the accuracy of the generated estimates is influenced by numerous complicating factors, some of which are difficult to assess while others may still be unknown to us. However, theory and application are inextricably linked and each benefits from the other. It is for this reason, for example, that the most widely used vorticity methods, such as those utilizing rigid porphyroclasts and quartz *c*-axis fabrics, appear to have more uncertainties and even pitfalls than other methods. For these methods, many of the sources of uncertainty/error have been identified by analyses in naturally deformed rocks. Moreover, analytical modelling by itself is doomed to perish without application to real rock deformation.

Obviously, an optimistic approach cannot overcome the uncertainties associated with the different vorticity methods. These problems can be significantly alleviated by applying as many methods as possible on a given sample. Agreement between different methods that record approximately the same part of deformation history of a shear zone provides evidence that the vorticity estimates are not merely artefacts of the assumptions underlying each method. The application of a number of methods with the same or different strain memory seems to be also an effective and promising way for evaluating the temporal and spatial variation of vorticity within naturally occurring shear zones. Some attempts have been made in this direction, especially in the last ten years, but much further work is required. A challenge for future work is to investigate whether shear zones in different tectonic regimes have different "vorticity signatures" in terms of spatio-temporal variation.

Thus, we now need more high quality vorticity studies in shear zones of various scales and tectonic environments. It is my belief that such studies will be able to provide robust data on critical topics such as the likely sources of errors of vorticity estimates, the strain memory of different methods, the descriptive power of methods for identifying triclinic flows, and the flow path in shear zones. Such data will provide valuable inputs for future analytical, numerical and experimental studies and that will, in turn, improve the existing methods and help to develop new ones, which minimize assumptions. Moreover, future work should be focussed on error and sensitivity analysis, which are currently limited in the literature. Until then, vorticity estimates obtained by the existing available methods should be used with caution.

Acknowledgements

I would like to thank the journal's editors for the invitation to prepare this review and especially Bill Dunne for his meticulous editorial work and valuable suggestions. Critical reviews by Rick Law and Scott Johnson were very helpful in improving the manuscript and are highly appreciated. Thanks also due to Tim Horscroft for editorial guidance. I dedicate this paper to young geoscientists who feel themselves steady enough to enter in this vortex.

Appendix. Supplementary data

The supplementary data associated with this article can be found, in the on-line version, at doi:10.1016/j.jsg.2010.08.009.

References

Bailey, C.M., Eyster, E.L., 2003. General shear deformation in the Pinaleno Mountains metamorphic core complex, Arizona. Journal of Structural Geology 25, 1883–1893.
Bailey, C.M., Francis, B.E., Fahrney, E.E., 2004. Strain and vorticity analysis of transpressional high-strain zones from the Virginia Piedmont, USA. In: Aslop, G.I., Holdsworth, R.E., McCaffrey, K.J.H., Hand, M. (Eds.), Flow Processes in Faults and Shear Zones. Geological Society, London, Special Publications, vol. 224, pp. 249–264.
Bailey, C.M., Polvi, L.E., Forte, A.M., 2007. Pure shear dominated high-strain zones in basement terranes. Geological Society of America Memoir 200, 93–108.
Beam, E.C., Fisher, D.M., 1999. An estimate of kinematic vorticity from rotated elongate porphyroblasts. Journal of Structural Geology 21, 1553–1559.
Behrmann, J.H., 1987. A precautionary note on shear bands as kinematic indicators. Journal of Structural Geology 9, 659–666.
Bell, T.H., Johnson, S.E., 1989. Porphyroblast inclusion trails: the key to orogenesis. Journal of Metamorphic Geology 7, 279–310.
Bell, T.H., Newman, R., 2006. Appalachian orogenesis: the role of repeated gravitational collapse. In: Butler, R., Mazzoli, S. (Eds.), Styles of Continental Compression. Geological Society of America Special Paper 414, pp. 95–118.
Berthé, D., Choukroune, P., Gapais, D., 1979. Orthogneiss mylonite and non-coaxial deformation of granites: the example of the South Armorican shear zone. Journal of Structural Geology 1, 31–42.
Bobyarchick, A., 1986. The eigenvalues of steady state flow in Mohr space. Tectonophysics 122, 35–51.
Bons, P.D., Jessell, M.W., Griera, A., 2009. Porphyroblast rotation versus nonrotation: conflict resolution!: comment. Geology 37, e182. doi:10.1130/G25131C.1.
Bouchez, J.L., Duval, P., 1982. The fabric of polycrystalline ice deformed in simple shear: experiments in torsion, natural deformation and geometrical interpretation. Textures and Microstructures 5, 171–190.
Burg, J.P., 1986. Quartz shape fabric variations and *c*-axis fabrics in a ribbon-mylonite: arguments for an oscillating foliation. Journal of Structural Geology 8, 123–131.
Carosi, R., Montomoli, C., Rubatto, D., Visona, D., 2006. Normal-sense shear zones in the core of the Higher Himalayan crystallines (Bhutan Himalaya): evidence for extrusion? In: Law, R.D., Searle, M.P., Godin, L. (Eds.), Channel Flow, Ductile Extrusion, and Exhumation in Continental Collision Zones Geological Society, London, Special Publications, vol. 268, pp. 425–444.
Ceriani, S., Mancktelow, N.S., Pennacchioni, G., 2003. Analogue modelling of the influence of shape and clast/matrix interface lubrication on the rotational behaviour of rigid clasts in simple shear. Journal of Structural Geology 25, 2005–2021.
Coelho, S., Passchier, C., 2008. Mohr-cyclides, a 3D representation of geological tensors: the examples of stress and flow. Journal of Structural Geology 30, 580–601.
Coelho, S., Passchier, C.W., Grasemann, B., 2005. Geometric description of flanking structures. Journal of Structural Geology 27, 597–606.
Czeck, D.M., Hudleston, P.J., 2003. Testing models for obliquely plunging lineations in transpression: a natural example and theoretical discussion. Journal of Structural Geology 25, 959–982.
Daczko, N.R., Klepeis, K.A., Clarke, G.L., 2001. Evidence of Early Cretaceous collisional-style orogenesis in northern Fiordland, New Zealand and its effects on the evolution of the lower crust. Journal of Structural Geology 23, 693–713.
Dell'Angelo, L.N., Tullis, J., 1989. Fabric development in experimentally sheared quartzites. Tectonophysics 169, 1–21.
De Paor, D.G., 1983. Orthographic analysis of geological structures – I. Deformation theory. Journal of Structural Geology 5, 255–277.
De Paor, D.G., 1994. The role of asymmetry in the formation of structures. Journal of Structural Geology 16, 467–475.
De Paor, D.G., Means, W.D., 1984. Mohr circles of the first and second kind and their use to represent tensor operations. Journal of Structural Geology 6, 693–701.
Ebner, M., Grasemann, B., 2006. Divergent and convergent non-isochoric deformation. Journal of Structural Geology 28, 1725–1733.
Ebner, M., Koehn, D., Toussaint, R., Renard, F., Schmittbuhl, J., 2009. Stress sensitivity of stylolite morphology. Earth and Planetary Science Letters 277, 394–398.
Etchecopar, A., Vasseur, G., 1987. A 3-D kinematic model of fabric development in polycrystalline aggregates: comparisons with experimental and natural examples. Journal of Structural Geology 9, 705–717.
Fay, C., Bell, T.H., Hobbs, B.E., 2009. Porphyroblast rotation versus nonrotation: conflict resolution!: reply. Geology 37, e188. doi:10.1130/G25630Y.1.
Fernández, C., Díaz-Azpiroz, M., 2009. Triclinic transpression zones with inclined extrusion. Journal of Structural Geology 31, 1255–1269.
Forte, A.M., Bailey, C.M., 2007. Testing the utility of the porphyroclast hyperbolic distribution method of kinematic vorticity analysis. Journal of Structural Geology 29, 983–1001.
Fossen, H., Tikoff, B., 1993. The deformation matrix for simultaneous simple shearing, pure shearing and volume change, and its application to transpression-transtension tectonics. Journal of Structural Geology 15, 413–422.

Fossen, H., Tikoff, B., 1997. Forward modelling of non-steady-state deformations and the 'minimum strain path'. Journal of Structural Geology 19, 987–996.
Frassi, C., Carosi, R., Montomoli, C., Law, R.D., 2009. Kinematics and vorticity of flow associated with post-collisional oblique transpression in the Variscan Inner Zone of northern Sardinia (Italy). Journal of Structural Geology 31, 1458–1471.
Ghosh, S.K., 1987. Measure of non-coaxiality. Journal of Structural Geology 9, 111–113.
Ghosh, S.K., Ramberg, H., 1976. Reorientation of inclusions by combination of pure shear and simple shear. Tectonophysics 34, 1–70.
Giorgis, S., Tikoff, B., 2004. Constraints on kinematics and strain from feldspar porphyroclast populations. In: Aslop, G.I., Holdsworth, R.E., McCaffrey, K.J.H., Hand, M. (Eds.), Flow Processes in Faults and Shear Zones. Geological Society, London, Special Publications, vol. 224, pp. 265–285.
Gomez-Rivas, E., Bons, P.D., Griera, A., Carreras, J., Druguet, E., Evans, L., 2007. Strain and vorticity analysis using small-scale faults and associated drag folds. Journal of Structural Geology 29, 1882–1899.
Grasemann, B., Stüwe, K., 2001. The development of flanking folds during simple shear and their use as kinematic indicators. Journal of Structural Geology 23, 715–724.
Grasemann, B., Edwards, M.A., Wiesmayr, G., 2006. Kinematic dilatancy effects on orogenic extrusion. In: Law, R.D., Searle, M.P., Godin, L. (Eds.), Channel Flow, Ductile Extrusion, and Exhumation in Continental Collision Zones. Geological Society, London, Special Publications, vol. 268, pp. 183–199.
Grasemann, B., Fritz, H., Vannay, J.C., 1999. Quantitative kinematic flow analysis from the main central thrust zone (NW-Himalaya, India): implications for a decelerating strain path and the extrusion of orogenic wedges. Journal of Structural Geology 21, 837–853.
Grasemann, B., Stüwe, K., Vannay, J.C., 2003. Sense and non-sense of shear in flanking structures. Journal of Structural Geology 25, 19–34.
Grujic, D., Casey, M., Davidson, C., Hollister, L.S., Kundig, R., Pavlis, T., Schmid, S., 1996. Ductile extrusion of the higher Himalayan crystalline in Bhutan: evidence from the quartz microfabrics. Tectonophysics 260, 21–43.
Heilbronner, R., Tullis, J., 2006. Evolution of *c*-axis pole figures and grain size during dynamic recrystallization: results from experimentally sheared quartzite. Journal of Geophysical Research 111, B10202.
Herwegh, M., Handy, M.R., 1996. The evolution of high temperature mylonitic microfabrics: evidence for simple shearing of a quartz analogue (norcamphor). Journal of Structural Geology 18, 689–710.
Herwegh, M., Handy, M.R., 1998. The origin of shape preferred orientations in mylonite: inferences from in-situ experiments on polycrystalline norcamphor. Journal of Structural Geology 20, 681–694.
Holcombe, R.J., Little, T.A., 2001. A sensitive vorticity gauge using rotated porphyroblasts, and its application to rocks adjacent to the Alpine Fault, New Zealand. Journal of Structural Geology 23, 979–989.
Hutton, D.H.W., 1982. A tectonic model for the emplacement of the main Donegal granite, NW Ireland. Journal of the Geological Society, London 139, 615–631.
Iacopini, D., Carosi, R., Xypolias, P., 2010. Implications of complex eigenvalues in homogeneous flow: a three-dimensional kinematic analysis. Journal of Structural Geology 32, 93–106.
Iacopini, D., Carosi, R., Montomoli, C., Passchier, C.W., 2008. Strain analysis and vorticity of flow in the Northern Sardinian Variscan Belt: recognition of a partitioned oblique deformation event. Tectonophysics 446, 77–96.
Iacopini, D., Passchier, C.W., Koehn, D., Carosi, R., 2007. Fabric attractors in general triclinic flow systems and their application to high strain shear zones: a dynamical system approach. Journal of Structural Geology 29, 298–317.
Ishii, K., 1992. Partitioning of non-coaxiality in deforming layered rock masses. Tectonophysics 210, 33–43.
Jeffery, G.B., 1922. The motion of ellipsoidal particles immersed in a viscous fluid. Proceedings of the Royal Society, London A102, 161–179.
Jessell, M., Lister, G.S., 1990. A simulation of the temperature dependence of quartz fabrics. In: Knipe, R.J., Rutter, E.H. (Eds.), Deformation Mechanisms, Rheology and Tectonics. Geological Society, London, Special Publications, vol. 54, pp. 353–362.
Jessup, M.J., Law, R.D., Frassi, C., 2007. The rigid grain net (RGN): an alternative method for estimating mean kinematic vorticity number (W_m). Journal of Structural Geology 29, 411–421.
Jessup, M.J., Law, R.D., Searle, M.P., Hubbard, M.S., 2006. Structural evolution and vorticity of flow during extrusion and exhumation of the Greater Himalayan Slab, Mount Everest Massif, Tibet/Nepal: implications for orogen-scale flow partitioning. In: Law, R.D., Searle, M.P., Godin, L. (Eds.), Channel Flow, Ductile Extrusion, and Exhumation in Continental Collision Zones. Geological Society, London, Special Publications, vol. 268, pp. 379–414.
Jiang, D., 1994. Flow variation in layered rocks subjected to bulk flow of various kinematic vorticities: theory and geological implications. Journal of Structural Geology 16, 1159–1172.
Jiang, D., 1999. Vorticity decomposition and its application to sectional flow characterization. Tectonophysics 301, 243–259.
Jiang, D., Williams, P.F., 1998. High-strain zones: a unified model. Journal of Structural Geology 20, 1105–1120.
Jiang, D., Lin, S., Williams, P.F., 2001. Deformation paths in high-strain zones, with reference to slip partitioning in transpressional plate-boundary regions. Journal of Structural Geology 23, 991–1005.
Johnson, S.E., 2009. Porphyroblast rotation and strain localization: debate settled! Geology 37, 663–666.
Johnson, S.E., Lenferink, H.J., Price, N.A., Marsh, J.H., Koons, P.O., West Jr., D.P., Beane, R., 2009a. Clast-based kinematic vorticity gauges: the effects of slip at matrix/clast interfaces. Journal of Structural Geology 31, 1322–1339.
Johnson, S.E., Lenferink, H.J., Marsh, J.H., Price, N.A., Koons, P.O., West Jr., D.P., 2009b. Kinematic vorticity analysis and evolving strength of mylonitic shear zones: new data and numerical results. Geology 37, 1075–1078.
Jones, R.R., Holdsworth, R.E., 1998. Oblique simple shear in transpression zones. In: Holdsworth, R.E., Strachan, R.A., Dewey, J.F. (Eds.), Continental Transpressional and Transtensional Tectonics. Geological Society, London, Special Publications, vol. 135, pp. 35–40.
Klepeis, K.A., Daczko, N.R., Clarke, G.L., 1999. Kinematic vorticity and tectonic significance of superposed mylonites in a major lower crustal shear zone, northern Fiordland, New Zealand. Journal of Structural Geology 21, 1385–1406.
Knipe, R.J., White, S.H., 1979. Deformation in low grade shear zones in the Old Red Sandstone, S.W. Wales. Journal of Structural Geology 1, 53–66.
Knipe, R.J., Law, R.D., 1987. The influence of crystallographic orientation and grain boundary migration on microstructural and textural development in a S-C mylonite. Tectonophysics 135, 155–169.
Kocher, T., Mancktelow, N.S., 2006. Flanking structure development in anisotropic viscous rock. Journal of Structural Geology 28, 1139–1145.
Kuiper, Y.D., Jiang, D., 2010. Kinematics of deformation constructed from deformed planar and linear elements: the method and its application. Tectonophysics. doi:10.1016/j.tecto.2010.06.009.
Kumerics, C., Ring, U., Brichau, S., Glodny, J., Monié, P., 2005. The extensional Messaria shear zone and associated brittle detachment faults, Aegean Sea, Greece. Journal of the Geological Society, London 162, 701–721.
Kurz, G.A., Northrup, C.J., 2008. Structural analysis of mylonitic fault rocks in the Cougar Creek Complex, Oregon–Idaho using the porphyroclast hyperbolic distribution method, and potential use of SC′-type extensional shear bands as quantitative vorticity indicators. Journal of Structural Geology 30, 1005–1012.
Langille, L., Jessup, M.J., Cottle, J.M., Newell, D., Seward, G., 2010. Kinematic evolution of the Ama Drime detachment: Insights into orogen-parallel extension and exhumation of the Ama Drime Massif, Tibet-Nepal. Journal of Structural Geology 32, 900–919.
Larson, K.P., Godin, L., 2009. Kinematics of the Greater Himalayan sequence, Dhaulagiri Himal: implications for the structural framework of central Nepal. Journal of the Geological Society, London 166, 25–43.
Law, R.D., 1990. Crystallographic fabrics: a selective review of their applications to research in structural geology. In: Knipe, R.J., Rutter, E.H. (Eds.), Deformation Mechanisms, Rheology and Tectonics. Geological Society, London, Special Publications, vol. 54, pp. 335–352.
Law, R.D., 2010. Moine thrust zone mylonites at the Stack of Glencoul: II – results of vorticity analyses and their tectonic significance. In: Law, R.D., Butler, R.W.H., Holdsworth, R.E., Krabbendam, M., Strachan, R.A. (Eds.), Continental Tectonics and Mountain Building: The Legacy of Peach and Horne. Geological Society, London, Special Publications, vol. 335, pp. 579–602.
Law, R.D., Casey, M., Knipe, R.J., 1986. Kinematic and tectonic significance of microstructures and crystallographic fabrics within quartz mylonites from the Assynt and Eriboll regions of the Moine thrust zone, NW Scotland. Transactions of the Royal Society of Edinburgh: Earth Sciences 77, 99–126.
Law, R.D., Knipe, R.J., Dayan, H., 1984. Strain-path partitioning within thrust sheets: microstructural and petrofabric evidence from the Moine thrust zone at Loch Eriboll, northwest Scotland. Journal of Structural Geology 6, 477–497.
Law, R.D., Schmid, S.M., Wheeler, J., 1990. Simple shear deformation and quartz crystallographic fabrics: a possible natural example from the Torridon area of NW Scotland. Journal of Structural Geology 12, 29–45.
Law, R.D., Searle, M.P., Simpson, R.L., 2004. Strain, deformation temperatures and vorticity of flow at the top of the greater Himalayan Slab, Everest Massif, Tibet. Journal of the Geological Society, London 161, 305–320.
Lin, S., Jiang, D., Williams, P.F., 1998. Transpression (or transtension) zones of triclinic symmetry: natural example and theoretical modelling. In: Holdsworth, R.E., Strachan, R.A., Dewey, J.F. (Eds.), Continental Transpressional and Transtensional Tectonics. Geological Society, London, Special Publications, vol. 135, pp. 41–58.
Lisle, R.J., 1994. Palaeostrain analysis. In: Hancock, P.L. (Ed.), Continental Deformation. Pergamon Press, Oxford, pp. 28–42.
Lister, G.S., Hobbs, B.E., 1980. The simulation of fabric development during plastic deformation and its application to quartzite: the influence of deformation history. Journal of Structural Geology 2, 355–370.
Lister, G.S., Snoke, A.W., 1984. S-C mylonites. Journal of Structural Geology 6, 617–638.
Lister, G.S., Williams, P.F., 1983. The partitioning of deformation in flowing rock masses. Tectonophysics 92, 1–33.
Malvern, L.E., 1969. Introduction to the Mechanics of a Continuous Medium. Prentice-Hall, Englewood Cliffs, New Jersey.
Mancktelow, N.S., Visser, P., 1993. The rotation of garnet porphyroblasts around a single fold, Lukmanier Pass, Central Alps: reply. Journal of Structural Geology 15, 1369–1372.
Marques, F.O., Coelho, S., 2003. 2D shape preferred orientations of rigid particles in transtensional viscous flow. Journal of Structural Geology 25, 841–854.
Marques, F.O., Burlini, L., 2008. Rigid inclusions rotate in geologic materials as shown by torsion experiments. Journal of Structural Geology 30, 1368–1371.
Marques, F.O., Schmid, D.W., Andersen, T.B., 2007. Applications of inclusion behaviour models to a major shear zone system: the Nordfjord-Sogn Detachment Zone in Western Norway. Journal of Structural Geology 29, 1622–1631.
Masuda, T., Michibayashi, K., Ohta, H., 1995. Shape preferred orientation of rigid particles in a viscous matrix: reevaluation to determine kinematic parameters of ductile deformation. Journal of Structural Geology 17, 115–129.

McKenzie, D., 1979. Finite deformation during fluid flow. Geophysical Journal of the Royal Astronomical Society 58, 689–715.
Means, W.D., 1981. The concept of steady – state foliation. Tectonophysics 78, 179–199.
Means, W.D., 1982. An unfamiliar Mohr circle construction for finite strain. Tectonophysics 89, T1–T6.
Means, W.D., 1983. Application of the Mohr-circle construction to problems of inhomogeneous deformation. Journal of Structural Geology 5, 279–286.
Means, W.D., 1989. Stretching faults. Geology 17, 893–896.
Means, W.D., 1994. Rotational quantities in homogeneous flow and the development of smallscale structure. Journal of Structural Geology 16, 437–445.
Means, W.D., Hobbs, B.E., Lister, G.S., Williams, P.F., 1980. Vorticity and non-coaxiality in progressive deformations. Journal of Structural Geology 2, 371–378.
Mulchrone, K.F., 2007. An analytical solution in 2D for the motion of rigid elliptical particles with a slipping interface under a general deformation. Journal of Structural Geology 29, 950–960.
Mulchrone, K.F., Grogan, S., De, P., 2005. The relationship between magmatic tiling, fluid flow and crystal fraction. Journal of Structural Geology 27, 179–197.
Northrup, C.J., 1996. Structural expressions and tectonic implications of general non-coaxial flow in the midcrust of a collisional orogen: the northern Scandinavian Caledonides. Tectonics 15, 490–505.
Oesterling, N., Heilbronner, R., Stünitz, H., Barnhoorn, A., Molli, G., 2007. Strain dependent variation of microstructure and texture in naturally deformed Carrara marble. Journal of Structural Geology 29, 681–696.
Passchier, C.W., 1986. Flow in natural shear zones – the consequences of spinning flow regimes. Earth and Planetary Science Letters 77, 70–80.
Passchier, C.W., 1987a. Stable positions of rigid objects in non-coaxial flow – a study in vorticity analysis. Journal of Structural Geology 9, 679–690.
Passchier, C.W., 1987b. Efficient use of the velocity gradients tensor in flow modelling. Tectonophysics 136, 159–163.
Passchier, C.W., 1988a. The use of Mohr circles to describe non-coaxial progressive deformation. Tectonophysics 149, 323–338.
Passchier, C.W., 1988b. Analysis of deformation paths in shear zones. Geologische Rundschau 77, 309–318.
Passchier, C.W., 1990a. A Mohr circle construction to plot the stretch history of material lines. Journal of Structural Geology 12, 513–515.
Passchier, C.W., 1990b. Reconstruction of deformation and flow parameters from deformed vein sets. Tectonophysics 180, 185–199.
Passchier, C.W., 1991. The classification of dilatant flow types. Journal of Structural Geology 13, 101–104.
Passchier, C.W., 1997. The fabric attractor. Journal of Structural Geology 19, 113–127.
Passchier, C.W., 1998. Monoclinic model shear zones. Journal of Structural Geology 20, 1121–1137.
Passchier, C.W., 2001. Flanking structures. Journal of Structural Geology 23, 951–962.
Passchier, C.W., Coelho, S., 2006. An outline of shear-sense analysis in high-grade rocks. Gondwana Research 10, 66–76.
Passchier, C.W., Trouw, R.A.J., 2005. Microtectonics, second ed. Springer Verlag, Berlin.
Passchier, C.W., Urai, J.L., 1988. Vorticity and strain analysis using Mohr diagrams. Journal of Structural Geology 10, 755–763.
Passchier, C.W., Trouw, R.A.J., Zwart, H.J., Vissers, R.L.M., 1992. Porphyroblast rotation: eppur si muove? Journal of Metamorphic Geology 10, 283–294.
Platt, J.P., Behrmann, J.H., 1986. Structures and fabrics in a crustal scale shear zone, Betic Cordilleras, S.E. Spain. Journal of Structural Geology 8, 15–34.
Platt, P.P., Vissers, R.L.M., 1980. Extensional structures in anisotropic rocks. Journal of Structural Geology 2, 397–410.
Pray, J.R., Secor Jr., D.T., Sacks, P.E., Maher Jr., H.D., 1997. Rotation of fabric elements in convergent shear zones, with examples from the southern Appalachians. Journal of Structural Geology 19, 1023–1036.
Ramberg, H., 1975. Particle paths, displacement and progressive strain applicable to rocks. Tectonophysics 28, 1–37.
Ramsay, J.G., 1980. Shear zone geometry: a review. Journal of Structural Geology 2, 83–101.
Ramsay, J.G., Graham, R.H., 1970. Strain variation in shear belts. Canadian Journal of Earth Sciences 7, 786–813.
Ramsay, J.G., Huber, M.I., 1983. The Techniques of Modern Structural Geology. In: Strain Analysis, vol. 1. Academic Press.
Ratschbacher, L., Wenk, H.-R., Sintubin, M., 1991. Calcite textures: examples from nappes with strain-path partitioning. Journal of Structural Geology 13, 369–384.
Ree, J.H., 1991. An experimental steady-state foliation. Journal of Structural Geology 13, 1001–1011.
Robin, P.Y.F., Cruden, A.R., 1994. Strain and vorticity patterns in ideally ductile transpression zones. Journal of Structural Geology 16, 447–466.
Sarkarinejad, K., Heyhat, M., Faghih, A., Kusky, T., 2010. Heterogeneous ductile deformation and quartz *c*-axis fabric development within the HP-LT Sanandaj-Sirjan Metamorphic Belt, Iran. Tectonophysics 485, 283–289.
Schoneveld, C., 1977. A study of some typical inclusion patterns in strongly paracrystalline-rotated garnets. Tectonophysics 39, 453–471.
Short, H.A., Johnson, S.E., 2006. Estimation of vorticity from fibrous calcite veins, central Maine, USA. Journal of Structural Geology 28, 1167–1182.
Simpson, C., De Paor, D.G., 1993. Strain and kinematic analysis in general shear zones. Journal of Structural Geology 15, 1–20.
Simpson, C., De Paor, D.G., 1997. Practical analysis of general shear zones using the porphyroclast hyperbolic distribution method: an example from the Scandinavian Caledonides. In: Sengupta, S. (Ed.), Evolution of Geological Structures in Micro- to Macro-Scales. Chapman and Hall, pp. 169–184.
Smith, J.V., Durney, D.W., 1992. Experimental formation of brittle structural assemblages in oblique divergence. Tectonophysics 216, 235–253.
Sullivan, W.A., 2008. Significance of transport-parallel strain variations in part of the Raft River shear zone, Raft River Mountains, Utah, USA. Journal of Structural Geology 30, 138–158.
Sullivan, W.A., 2009. Kinematic significance of L tectonites in the footwall of a major terrane-bounding thrust fault, Klamath Mountains, California, USA. Journal of Structural Geology 31, 1197–1211.
Sullivan, W.A., Law, R.D., 2007. Deformation path partitioning within the transpressional White Mountain shear zone, California and Nevada. Journal of Structural Geology 29, 583–598.
Takeshita, T., Wenk, H.R., Lebensohn, R., 1999. Development of preferred orientation and microstructure in sheared quartzite: comparison of natural data and simulated results. Tectonophysics 312, 133–155.
Talbot, C.J., 1970. The minimum strain ellipsoid using deformed quartz veins. Tectonophysics 9, 47–74.
Ten Brink, C.E., Passchier, C.W., 1995. Modelling of mantled porphyroclasts using non-Newtonian rock analogue materials. Journal of Structural Geology 17, 131–146.
Thigpen, J.R., Law, R.D., Lloyd, G.E., Brown, S.J., Cook, B., 2010a. Deformation temperatures, vorticity of flow and strain symmetry in the Loch Eriboll mylonites, NW Scotland: implications for the kinematic and structural evolution of the northernmost Moine thrust zone. In: Law, R.D., Butler, R.W.H., Holdsworth, R.E., Krabbendam, M., Strachan, R.A. (Eds.), Continental Tectonics and Mountain Building: The Legacy of Peach and Horne. Geological Society, London, Special Publications, vol. 335, pp. 623–662.
Thigpen, J.R., Law, R.D., Lloyd, G.E., Brown, S.J., 2010b. Deformation temperatures, vorticity of flow, and strain in the Moine thrust zone and Moine nappe: Reassessing the tectonic evolution of the Scandian foreland-hinterland transition zone. Journal of Structural Geology 32, 920–940.
Tikoff, B., Fossen, H., 1993. Simultaneous pure shear and simple shear: the unifying deformation matrix. Tectonophysics 217, 267–283.
Tikoff, B., Fossen, H., 1995. The limitations of three-dimensional kinematic vorticity analysis. Journal of Structural Geology 17, 1771–1784.
Tikoff, B., Teyssier, C., 1994. Strain and fabric based on porphyroclast interaction. Journal of Structural Geology 16, 477–491.
Truesdell, C., 1953. Two measures of vorticity. Journal of Rational Mechanics Analysis 2, 173–217.
Trullenque, G., Kunze, K., Heilbronner, R., Stünitz, H., Schmid, S.M., 2006. Microfabrics of calcite ultramylonites as records of coaxial and non-coaxial deformation kinematics: examples from the Rocher de l'Yret shear zone (Western Alps). Tectonophysics 424, 69–97.
Vissers, R.L.M., 1987. The effect of foliation orientation on the inferred rotation axes and rotation angles of rotated porphyroblasts. Tectonophysics 139, 275–283.
Vissers, R.L.M., 1989. Asymmetric quartz *c*-axis fabrics and flow vorticity: a study using rotated garnets. Journal of Structural Geology 11, 231–244.
Wallis, S.R., 1992. Vorticity analysis in a metachert from the Sanbagawa belt, SW Japan. Journal of Structural Geology 14, 271–280.
Wallis, S.R., 1995. Vorticity analysis and recognition of ductile extension in the Sanbagawa belt, SW Japan. Journal of Structural Geology 17, 1077–1093.
Wallis, S.R., Platt, J.P., Knott, S.D., 1993. Recognition of syn-convergence extension in accretionary wedges with examples from the Calabrian arc and the eastern Alps. American Journal of Science 293, 463–495.
Weijermars, R., 1991. The role of stress in ductile deformation. Journal of Structural Geology 13, 1061–1078.
Wells, M.L., 2001. Rheological control on the initial geometry of the Raft River detachment fault and shear zone, western United States. Tectonics 20, 435–457.
Wenk, H.R., Takeshita, T., Bechler, E., Erskine, B.G., Matthies, S., 1987. Pure shear and simple shear calcite textures. Comparison of experimental, theoretical and natural data. Journal of Structural Geology 9, 731–746.
Wiesmayr, G., Grasemann, B., 2005. Sense and non-sense of shear in flanking structures with layer-parallel shortening: implications for fault-related folds. Journal of Structural Geology 27, 249–264.
Williams, P.F., Jiang, D., 1999. Rotating garnets. Journal of Metamorphic Geology 17, 367–378.
Xypolias, P., 2009. Some new aspects of kinematic vorticity analysis in naturally deformed quartzites. Journal of Structural Geology 31, 3–10.
Xypolias, P., Doutsos, T., 2000. Kinematics of rock flow in a crustal-scale shear zone: implication for the orogenic evolution of the southwestern Hellenides. Geological Magazine 137, 81–96.
Xypolias, P., Kokkalas, S., 2006. Heterogeneous ductile deformation along a mid-crustal extruding shear zone: an example from the External Hellenides (Greece). In: Law, R.D., Searle, M.P., Godin, L. (Eds.), Channel Flow, Ductile Extrusion, and Exhumation in Continental Collision Zones. Geological Society, London, Special Publications, vol. 268, pp. 497–516.
Xypolias, P., Koukouvelas, I.K., 2001. Kinematic vorticity and strain rate patterns associated with ductile extrusion in the Chelmos Shear Zone (External Hellenides, Greece). Tectonophysics 338, 59–77.
Xypolias, P., Spanos, D., Chatzaras, V., Kokkalas, S., Koukouvelas, I., 2010. Vorticity of flow in ductile thrust zones: examples from the Attico-Cycladic Massif (Internal Hellenides, Greece). In: Law, R.D., Butler, R.W.H., Holdsworth, R.E., Krabbendam, M., Strachan, R.A. (Eds.), Continental Tectonics and Mountain Building: The Legacy of Peach and Horne. Geological Society, London, Special Publications, vol. 335, pp. 687–714.
Yamaji, A., 2008. Theories of strain analysis from shape fabrics: a perspective using hyperbolic geometry. Journal of Structural Geology 30, 1451–1465.